Decomposition of Poly(vinyl chloride) in Inductively Coupled Radiofrequency Thermal Plasma

Péter Fazekas*, Zsuzsanna Czégény, János Mink, Eszter Bódis, Szilvia Klébert, Csaba Németh, Anna Mária Keszler, Zoltán Károly, János Szépvölgyi

Institute of Materials and Environmental Chemistry, Research Centre for Natural Sciences, Hungarian Academy of Sciences. Magyar tudósok körútja 2, 1115 Budapest, Hungary.

*corresponding author's e-mail address: fazekas.peter@ttk.mta.hu

Keywords: Poly(vinyl chloride), Polymer Waste, Thermal Decomposition, Radiofrequency Thermal Plasma, Fourier Transform Infrared Spectroscopy, Gas Chromatography/Mass Spectrometry

Abstract

Decomposition of poly(vinyl chloride) (PVC) was studied in inductively coupled radiofrequency thermal plasma in neutral, oxidative and reductive conditions. The exhaust gases were analysed by Fourier transform infrared spectroscopy (FT-IR), and their main components were identified as CO, CO_2, C_2H_2, H_2O and HCl. The weaker bands in the infrared spectra were assigned by density function theory calculations and P-R separation method. The extent of PVC decomposition was calculated from the amount of solid soot, which was also studied by transmission electron microscopy (TEM) for morphology and composition. Organic compounds adsorbed on the surface of the soot were extracted by toluene and analysed by gas chromatography mass spectrometry (GC/MS). The extracts

comprised of various polycyclic aromatic hydrocarbons (PAHs) and their methylated and chlorinated derivatives. Their amount was greatly affected by the experimental conditions. The presence of oxygen decreased the formation of PAHs, while it increased the formation of polychlorinated PAH compounds. In the presence of hydrogen PAH formation was observed. However, dioxin or furan derivatives were not detected in the decomposition products.

1. Introduction

Poly(vinyl chloride) (PVC) is one of the most common polymeric material with a production of 38.5 million tons in 2013, which accounted for 12 % of the total plastic production worldwide. The demand for PVC is increasing, therefore production is forecasted to rise by 3.2 % per year by 2021 [1], due to the broad usage of PVC in many areas of everyday life, such as the building industry (doors, window frames, pipes, cables), computers (keyboards, cases, various peripheries), medical devices (blood and plasma bags), clothing (raincoats, imitation leathers, rubber boots), food packaging (containers, bottles) and in the administrative sector (credit cards, identity cards) [2]. In usual environmental conditions PVC is a stable material and is not prone to decomposition reactions. Only its grain size decreases due to physical weathering. After its lifespan the deposition of PVC in landfills requires more and more space, which means increasing environmental impacts and expenses. Therefore, development of reliable recycling or decomposition methods is an urgent necessity. Although several technologies have been proposed for recycling, they have not reached a commercially feasible solution yet [3]. Thermal degradation of PVC via conventional high temperature decomposition such as pyrolysis or cracking results in toxic by-products, which are stable and also present hazards both on human health and the environment. Significant amounts of

benzene and toluene are being formed on decomposition of PVC due to ring closing reactions taking place after the elimination of HCl from the polymer chain [4]. This can be modified by metals, metal oxides or other polymers [5-6]. In addition, the presence of PVC has remarkable impact on the decomposition of numerous plastics [6]. Thermal decomposition of PVC along with lignocellulose biomass materials results in significant formation of chloromethane [7]. During incineration of PVC formation of different types of dioxins and furans were also reported [8].

The inductively coupled thermal plasmas (IC-TPs), which are characterized by high temperature and energy density, contain photons, ground-state and excited atoms, ions and molecules. Due to their special properties IC-TPs offer an environmental benign solution for the destruction of organic materials and polymers, too. The extremely high temperature (8000–12000 K) and strong UV radiation facilitate decomposition and induce a large number of reactive species. The high quenching rate of gases (~10^6 K s^{-1}) is advantageous to avoid the recombination of radicals into large, stable molecules, like dioxins. Therefore, this technique has been increasingly applied in waste treatment, for example in the decomposition of chlorine-free polymers [9] and halogenated organic molecules [10-11], as well.

In this paper we report on the decomposition of PVC in IC-TP plasma in neutral, oxidative and reductive conditions. The decomposition process was characterized by the analysis of all gaseous, liquid and solid products. On the basis of experimental results, the most favourable conditions of PVC decomposition were determined in the particular system.

2. Materials and methods

In this study PVC powder, as a model, was applied free of additives, and was supplied by BorsodChem Co. (Hungary). The number average molar mass (M_n) was 28150 g mole^{-1}, its mass average molar mass (M_w) was 89660 g mole^{-1} and had an average particle size of 150 μm.

The experimental set-up consisted of an RF inductively coupled plasma torch (TEKNA PL-35) connected to a high frequency (4–5 MHz) LEPEL generator, a reactor, a cyclone, a filter unit and a vacuum pump. The PVC powder was fed axially into the hottest zone of the plasma column by a PRAXAIR powder feeder and an atomizer nozzle of 2.16 mm inner diameter. For the atomization Ar flow (99.996 % purity, Messer Hungarogáz Ltd.) of 9.4 dm^3 min^{-1} was used. The plasma torch was also operated with Ar central gas and sheath gas with flow rates of 15.5 and 35.5 dm^3 min^{-1}, respectively. In certain runs O_2 (99.5 %, Messer Hungarogáz Ltd.) or H_2 (99.98 %, Linde Gáz Magyarország Ltd.) was added into the sheath gas in different concentrations. The double-wall, water cooled cylindrical reactor shown in Figure 1, was made of stainless steel with the inner diameter of 19.7 cm and length of 121.6 cm. To determine the optimal conditions of decomposition, the following plasma parameters were changed in particular tests: (1) feeding rate of PVC (50–150 g h^{-1}), (2) oxygen and hydrogen concentration (in various stoichiometric ratios) and (3) plate power (15–25 kW). The experimental conditions are listed in Table 1. Stoichiometric ratios were calculated by assuming a complete oxidation (into CO_2, H_2O and HCl) and reduction (into CH_4 and HCl) of PVC, respectively. Tests designated as PVC1 and PVC2 stood for the blank samples of GC/MS measurements.

The exhaust gases were collected in a standard through-flow gas cell of 10 cm length equipped with KBr windows. Middle-infrared spectra (350-4000 cm^{-1}) were recorded by a Varian FTS-7000 high resolution (0.08 cm^{-1}) Fourier transform infrared spectrometer (FT-IR). The spectrometer had a dynamically aligned interferometer, a Peltier-thermostated

deutero triglycine sulphate (DTGS) detector and a high intensity ceramic source. 16 scans were accumulated from every sample with the resolution of 0.5 cm^{-1}. Quantitative analysis was done by the integration method using the Quasoft database, which contains the spectra of 250 small sized atmospheric contaminants with known concentration.

Density functional theory (DFT) calculations were used to define the fundamental frequencies, the IR and Raman intensities and the moments of inertia of expected acetylene derivatives. These calculations were carried out by the Gaussian 03 code. [12]

The solid soot was collected from the wall of the plasma reactor. Morphology of soot particles was characterized by transmission electron microscopy (TEM, Morgagni 268D). The specific surface area was measured by N_2 adsorption at 77 K using a 11-point BET method (Quantachrome, Autosorb-1).

Organic compounds adsorbed on the surface of the soot were ultrasonically extracted by toluene (Merck, HPLC grade purity). 10 mg soot was treated in 2 cm^3 toluene for 60 minutes. The extracts were analysed by GC/MS (Agilent Technologies Inc. 6890 GC/5973 MSD) using Agilent DB-1701 capillary column (30 m length, 0.25 mm inner diameter, 0.25 μm film thickness). 1 μl sample was injected to the column in splitless injection mode. Temperature of the GC injector was kept at 300 °C. The GC oven was hold at 50 °C for 1 min, and then increased to 280 °C at a rate of 10 °C min^{-1}. The mass spectrometer was operated at 70 eV in the electron impact ionisation mode. The mass detection ranged from 14 to 500 Da.

3. Results and Discussion

3.1 Analysis of the exhaust gases

3.1.1 Qualitative analysis

Decomposition of three PVC samples was studied by FT-IR; (1) pure PVC in Ar (PVC4), (2) pure PVC in O_2 (PVC9) and (3) pure PVC in H_2 (PVC13). The major components in the plasma gases were CO_2, CO, H_2O, C_2H_2 and HCl. All rotational-vibrational spectra of the small molecules are very different and very characteristic. The presence of oxygen containing species in neutral conditions can be explained by presence of oxygen traces of about 50 ppm in the Ar carrier, plasma and sheath gases.

Three well defined infrared bands of acetylene were observed at 729.7 (ν_5), 1326.4 ($\nu_4+\nu_5$) and 3287.3 (ν_3) cm^{-1} frequencies. The ν_5 refers to deformational (linear bending) mode of HCCH (perpendicular band) which exhibits P-, Q- and R-branches. The origin of the ν_5 band is at the maximum position of the Q-branch, which is illustrated in Figure 2. In contrast, the antisymmetric CH stretching (ν_3) is a so called parallel band exhibiting well separated P- and R-branches. In this case the band origin is in the middle of P- and R-branches, at 3287.3 cm^{-1} (Figure 3). Except the above discussed two fundamental modes (ν_3 and ν_5) there is another IR-active band exhibiting fine structure of parallel mode, which is a combination band of ν_4 and ν_5 fundamentals and detected at 1326.4 cm^{-1}. The ν_4 mode is only Raman active, observed at 611.8 cm^{-1} and its combination with ν_5 gives 1341.5 cm^{-1} which moves down to 1326.4 cm^{-1} due to an-harmonic vibrations.

Four well defined bands can be obtained in the IR spectrum of CO_2, at 667.6 (ν_2), 2348.7 (ν_3), 3616.2 ($2\nu_2+\nu_3$) and 3714.4 cm^{-1} ($\nu_1+\nu_3$). The bending mode (ν_2) exhibit P-, Q- and R-branches as perpendicular vibration. The antisymmetric CO_2 stretching (ν_3) has only P- and R-branches characteristic for bands of parallel vibrations (the induced dipole moment is parallel with the molecular axis). The two combination bands are also parallel modes with P- and R-branches.

The diatomic gas species (CO and HCl) both have one parallel fundamental mode with P- and R-branches.

The above described linear (C_2H_2, CO_2) and diatomic (CO, HCl) molecules gave rather similar band structures with P-, Q- and R-branches or with P- and R-branches. All these molecules have only one moment of inertia. But the H_2O as an asymmetric rotor has three different moment of inertia consequently exhibiting very complicated rotational fine structure, and even not easy to obtain the band origin. The three fundamentals obtained by theoretical analysis are at 1594.6 (ν_2), 3656.7 (ν_1) and 3755.8 (ν_3) cm^{-1} and a weak overtone is at 3154.4 ($2\nu_2$) cm^{-1}.

3.1.2 Quantitative analysis

Due to the rotational fine structure even the gas spectra of small molecules spread a broad range. This can lead to overlapping of bands of different molecules. Such a case is shown in Figure 4, where overtones of CO_2 overlap with OH stretching bands of H_2O. Similar situation was observed between deformation modes of C_2H_2 (ν_5) and CO_2 (ν_2) near 700 cm^{-1} (Figure 5). With careful spectral subtractions the effect of overlapping can be eliminated before concentration determination. Another problem is that the quantity of CO_2 and H_2O gases can always be determined with difficulties due to their permanent but variable presence in the atmosphere.

In Figure 6 the spectra of the pyrolysis products from PVC are shown. The library spectra of the main components, i.e. C_2H_2, HCl, CO and CO_2 were used for quantitative analysis. The results obtained by method of integration of experimental intensities are summarised in Table 2. Degradation of PVC in Ar produced large amount of hydrochloric acid (104.2 μmole dm^{-3}) and acetylene (38.6 μmole dm^{-3}).

In presence of hydrogen the decomposition results in smaller amount of HCl (30.6 μmole dm^{-3}). No CO formation was detected. However, presence of hydrogen has no effect on C_2H_2 formation of as its concentration does not change. The higher amount of CO_2 and the large concentration of H_2O may be attributed to the oxygen contamination of commercial hydrogen.

The decomposition process was more "complete" in the presence of oxygen, leading to CO_2, HCl and H_2O as main products.

3.1.3 Minor products

A more detailed analysis of IR spectra in Figure 6 refers to several additional weak bands. An extra overlapping band can be seen in the CH stretching region of acetylene in the high frequency side (Figure 7). The experimental spectrum 8a in Figure 7 showing the decomposition products of pure PVC contains not resolved extra bands at 3340 (R), 3332 (band origin) and 3323 (P) cm^{-1} (Figure 7 (8c)), which was obtained by subtraction of the spectrum of pure acetylene (Figure 7 (8b)).

Weak P- and R-branches were observed at 1248 and 1233 cm^{-1} with band origin at 1241.2 cm^{-1}, near the $\nu_4+\nu_5$ combination band (1326.9 cm^{-1}) of acetylene (Figure 8).

The strongest band in the region of C≡C–H deformation of acetylenes was observed at 628 cm^{-1} (Figure 9).

The above discussed three extra bands nicely correlate with the experimental IR data of di-acetylene (butadiene). The band origins at 3332, 1241 and 628 cm^{-1} [13] well correlate with our observations at 3332, 1241.2 and 628 cm^{-1} obtained in the sample of decomposition products of PVC. Our scaled DFT calculation gave 3341, 1294 and 628 cm^{-1}. The infrared active modes of di-acetylene are summarised in Table 3. The agreement of the wavenumbers

in the table is very good, but big discrepancies were observed between the experimental and the calculated band intensities.

The above assignments can be supported by the P-R band separation of di-acetylene. This method is used when bands of several molecules are very close to each other, therefore the assignation of the bands based on the spectral position is not possible. The well-known formula of band separation is given by Equation 1., as follows:

$$\Delta\nu_{\text{P-R}} = \left(\frac{8k}{hc}BT\right)^{0.5} = 2.3583(BT)^{0.5} \quad (1)$$

where $\Delta\nu_{\text{P-R}}$ is the value of the P-R separation, T is the absolute temperature, B is the rotational constant in cm^{-1} unit, k is the Boltzmann constant, h is the Planck constant and c is the velocity of light in vacuum [14]. In case of diacetylene B = 0.1326 cm^{-1} which gives $\Delta\nu_{\text{P-R}}$ = 14.9 cm^{-1}. In Table 3. the ν_4 band has 17 cm^{-1} and the $\nu_6+\nu_8$ combination band has 15.6 cm^{-1} P-R separations, which are agreed well with the theoretically predicted value. On the other hand, the calculated band separation of triacetylene (C_6H_2) is 8.5 cm^{-1} which is far from our experimental observations.

According to DFT calculation of polyacetylenes the IR active C≡C–H linear bending mode is expected at 729, 628, 617 and 616 cm^{-1} for C_2H_2, C_4H_2, C_6H_2 and C_8H_2, respectively. The weak bands in Figure 9 at 621.4 and 615.6 cm^{-1} may be assigned to trace amount of triacetylene and tetraacetylene, respectively. Unfortunately, it is difficult to assign the other weak bands in this region at 635, 634, 625 and 613 cm^{-1}.

The monochloroacetylene has a strong band at 607 cm^{-1}, which can be assigned to the lowest band at 613 cm^{-1}, but it also has another strong band at 2110 cm^{-1} which was not detected in our experiments [15].

3.2 Solid products analysis

In each test a black, solid soot, was collected from the reactor wall. Its yield from the decomposition was calculated according to Equation 2.:

$$\text{Soot yield} = \frac{\text{Amount of soot formed } (\text{g h}^{-1})}{\text{Carbon content of PVC fed } (\text{g h}^{-1})} \qquad (2)$$

Soot yields calculated by Eq. (2) are shown in Table 4. In Ar plasma the increase of plate power from 15 to 20 kW (PVC3 and PVC4) did not change the soot yield. However, at plate power of 25 kW (PVC5) the soot yield decreased by 8.6 % as compared to PVC4, which represents a relative decrease of about 25 %. The change in feed rate in the 50-150 g h^{-1} range did not show any effect on the soot yield. In the presence of oxygen increase of the plate power resulted in lower soot yield, most significantly at 25 kW (PVC8-10). Both sets of experiments, performed in Ar and in Ar+O_2, show that higher plate power leads to greater degree of gasification. Test with 1:2 oxygen/PVC stoichiometric ratio (PVC11) actually did not differ from that in neutral conditions (PVC4). In reductive conditions, applying Ar+H_2 plasma, soot formation decreased significantly as compared to neutral ones.

Specific surface area (SSA) of selected soot samples (Table 5.) varied in the range of 60 and 100 m^2 g^{-1}, which is typical for carbon blacks [16-17]. At the highest feed rate (PVC7) the low SSA value implies larger soot particles.

TEM micrographs of the soot samples depicted in Figure 10, show typical plate like particles with their size varied between 20-30 nm. Interestingly both in reductive and oxidative conditions, it increased to 40-50 nm in Ar+H_2 and to 60-80 nm in Ar+O_2. These values are in good agreement with our former results [18]. However, in neutral conditions the soot also contained particles with typical size of 200-1000 nm, which were identified as grains

of unreacted PVC (Figure 11). Therefore, for complete decomposition of PVC, oxidative or reductive conditions are required in the particular experimental system. In oxidative conditions the oxygen attacks the polymer chain, while hydrogen improves the heat transfer between the plasma flame and PVC particles due to its higher heat conductivity as compared to argon.

Based on the results of Japanese researchers [19] we also investigated possible the formation of graphene in the applied conditions. No specific G or 2D peaks of graphene at 1580 and 2700 cm^{-1} [20], respectively were detected in the Raman spectra of sample from Runs PVC4, 7, 9 and 14.

3.3 Analysis of extracts from the soot

3.3.1 Qualitative analysis of organic compounds extracted from the soot

The organic compounds adsorbed on the surface of the soot were extracted by toluene. The extracts were analysed by GC/MS, and the identified compounds are listed in Table 6.

With the exception of the linear hexachlorobutadiene all identified compounds were aromatic or polyaromatic hydrocarbons (PAH) and their methylated or chlorinated derivatives. Diacetylene and triacetylene, as probable building blocks of PAHs before the ring closing reactions, were detected in the gas phase by FT-IR. We did not detect any dioxins or furans, the only oxygen containing molecule was benzaldehyde.

In the presence of hydrogen we could observe only a slight change in the composition of the PAHs: the concentration of dimethylbiphenyl decreased below the detection limit. By contrast, the oxidative atmosphere had huge impact on the formation of by-products. Six compounds could not be detected, amongst them indenophenanthrene and benzoperylene

were the largest non-chlorinated molecules in the extracts, three (dimethylphenanthrene, phenylmethylnaphthalene, methylchrysene) were methylated PAH molecule and terphenyl was a three ring PAH. The oxygen reacts with the C_2 and CH radicals, which are the building blocks of polycyclic hydrocarbons. By decreasing the concentration of these radicals, the formation of larger molecules is less probable. Another effect of the oxygen was the appearance of polychlorinated PAHs, such as hexachlorobenzene or octochloronaphthalene. Several monochlorinated compounds have been identified under neutral conditions (chloronaphthalene, chloroanthracene, chloropyrene), which is in agreement with the literature [21], but higher degree of chlorination occurred only in oxidative conditions. We detected mainly the polychlorinated derivatives of benzene and naphthalene, even their perchlorinated variants. Hexachlorobutadiene was also detected, which is a fully chlorinated linear molecule. In view of our previous work [18], presence of such type of molecules was unexpected, but other papers confirm the possibility of its formation from chlorinated linear hydrocarbons in IC-TP plasmas [11]. This enhanced chlorination process can be attributed to the reaction between HCl and OH (Equation 3):

$$HCl + OH = H_2O + Cl \quad (3)$$

which is a well-established reaction in stratospheric chemistry [22]. The presence of the two precursors is known from the FT-IR data and our former optical emission measurements as well [23]. The newly formed chlorine radical attacks the aromatic rings and substitutes a hydrogen atom. Due to the large number of chlorine radicals this process leads to polychlorination [24].

3.3.2 Quantitative analysis of organic compounds extracted from the soot

Five different sets in the experimental conditions were investigated: the effect of plate power (1) and feed rate (2) under neutral condition, the effect of plate power (3) and stoichiometric ratio (4) in oxidative atmosphere and the effect of stoichiometric ratio (5) in the presence of hydrogen. The extracts consisted mostly of three and four ring molecules in each condition.

The influence of plate power under neutral condition showed controversial impact. The increase from 15 to 20 kW resulted in a significant decrease in the concentration of the PAH compounds in every ring number category, however at 25 kW the concentrations started to rise in small extent (Figure 12a).

Higher feed rates resulted in higher PAH concentrations (Figure 12b). The higher amount of material in the plasma flame reduced the specific energy and that lower amount was not sufficient to prevent the recombination of the larger number of fragments into larger molecules.

The influence of plate power on the concentrations of PAHs in oxidative atmosphere was similar as it was found in the absence of oxygen (Figure 12c). Increasing it from 15 to 20 kW resulted a slight decrease in concentrations, but in a much lower degree than in case of neutral atmosphere. At 25 kW the two ring molecules decreased, but the concentrations of the three and for ring compound increased higher than at 15 kW. However, the effect of oxygen was significant, the PAH concentrations were one order of magnitude lower than in neutral environment. Furthermore, as mentioned above, the largest, six ring molecules disappeared completely, while one ring compounds were detected only in oxidative conditions.

Increasing the oxygen content to the 1:1 stoichiometric ratio resulted an obvious drop in the concentration of the PAH molecules (Figure 12d). At 1:2 ratio the soot yield was not different from the neutral condition (Table 4.) which showed that the oxygen reacted with the

HCl instead of the carbon. The appearance of the polychlorinated compounds supports this theory (Figure 13). At higher oxygen rates their concentrations dropped because the increased amount of oxygen was able to react with the building aromatic rings.

The reductive environment was detrimental to the decomposition process. The presence of hydrogen increased the amount of PAH compounds at every stoichiometric rate (Figure 12e). The hydrogen did not react with the small carbon molecules and fragments, like C_2, and CH, to form stable gaseous hydrocarbons, instead assisted in the formation of largerthe enlargement and enrichment of the PAHs.

4. Conclusions

In this study PVC powder was used as a model compound to reveal the decomposition processes of such type of halogenated polymers in inductively coupled radiofrequency thermal plasma. TEM analysis of the solid products revealed that the decomposition of PVC was not complete in Ar plasma, therefore addition of auxiliary gases, such as oxygen or hydrogen is required.

The exhaust gases from the plasma reactor mainly consist of acetylene, hydrogen chloride, carbon dioxide, carbon monoxide and water vapour. Different polyacetylenes, the building blocks of the PAHs were also detected in the gaseous products.

Formation of a large number of different polyaromatic hydrocarbons could be detected by the analysis of soot. As they have adverse effect on the environment and human health so their formation should be minimized. Their analysis revealed some important tendencies, which should be taken into account in designing the decomposition process. Increased feed rate leads to higher PAH formation. Therefore, the emission thresholds of PVC

decomposition must be monitored closely. According to our findings, higher plate power does not result in more complete decomposition. Thus, it is not necessary to operate the plasma generator with maximum plate power in particular conditions. Presence of oxygen hinders formation of PAHs. On the other hand, in the absence of oxygen no polychlorinated PAHs are formed. Hydrogen increases formation of PAHs, especially those with higher ring numbers, therefore its presence is detrimental.

Acknowledgement: This work has been supported by the National Development Agency of Hungary (Grant No. KTIA_AIK_12-1-2012-0004).

References

1. Yu, J.; Sun, L.; Ma, C.; Qiao, Y.; Yao, H. (2016): Thermal degradation of PVC: A review. Waste Management 48, 300-314.
2. Moulay, S. (2010): Chemical modification of poly(vinyl chloride)-Still on the run. Progress in Polymer Science 35, 303-331.
3. Shadat-Sojai, M.; Bekhschandeh, G.-R. (2011): Recycling of PVC wastes. Polymer Degradation and Stability 96, 404-415.
4. Miranda, R.; Yang, J.; Roy, C.; Vasile, C. (1999): Vacuum Pyrolysis of PVC I. Kinetic study. Polymer Degradation and Stability 64, 127-144.
5. Blazsó M.; Jakab E. (1999): Effect of metals, metal oxides and carboxylates on the thermal decomposition processes of poly (vinyl chloride). Journal of Analytical and Applied Pyrolysis 49, 125-143.
6. Czégény Zs.; Jakab E.; Blazsó M. (2002): Thermal decomposition of polymer mixtures containing poly (vinyl chloride). Macromolecular Materials and Engineering 287, 277-284.

7. Czégény Zs.; Jakab E.; Bozi J.; Blazsó M. (2015): Formation of chloromethane from lignocellulosic materials in the presence of PVC. Journal of Analytical and Applied Pyrolysis 113, 123-132.
8. Christmann, W.; Kasiske, D.; Klöppel, K. D.; Partscht, H.; Rotard, W. (1989): Combustion of polyvinylchloride- an important source for the formation of PCDD/PCDF. Chemosphere 19, 387-392.
9. Gudetti, R. R.; Knight, R.; Grossmann, E. D. (2000): Depolymerization of polyethylene using induction-coupled plasma technology. Plasma Chemistry and Plasma Processing 20, 37-64.
10. Főglein K. A.; Szépvölgyi J.; Szabó T. P.; Mészáros E.; Jakab E.; Babievskaya, I. Z.; Mohai I.; Károly Z. (2005): Comparative study on decomposition of $CFCl_3$ in thermal and cold plasma. Plasma Chemistry and Plasma Processing 25, 275-288.
11. Főglein K. A.; Szabó P. T.; Babievskaya, I. Z.; Szépvölgyi J. (2005): Comparative study on the decomposition of chloroform in thermal and cold plasma. Plasma Chemistry and Plasma Processing 25, 289-301.
12. Frisch, M. J.; Trucks, G. W.; Schlegel, H. B.; Scuseria, G. E.; Robb, M. A.; Cheeseman, J. R.; Montgomery, Jr., J. A.; Vreven, T.; Kudin, K. N.; Burant, J. C.; Millam, J. M.; Iyengar, S. S.; Tomasi, J.; Barone, V.; Mennucci, B.; Cossi, M.; Scalmani, G.; Rega, N.; Petersson, G. A.; Nakatsuji, H.; Hada, M.; Ehara, M.; Toyota, K.; Fukuda, R.; Hasegawa, J.; Ishida, M.; Nakajima, T.; Honda, Y.; Kitao, O.; Nakai, H.; Klene, M.; Li, X.; Knox, J. E.; Hratchian, H. P.; Cross, J. B.; Bakken, V.; Adamo, C.; Jaramillo, J.; Gomperts, R.; Stratmann, R. E.; Yazyev, O.; Austin, A. J.; Cammi, R.; Pomelli, C.; Ochterski, J. W.; Ayala, P. Y.; Morokuma, K.; Voth, G. A.; Salvador, P.; Dannenberg, J. J.; Zakrzewski, V. G.; Dapprich, S.; Daniels, A. D.; Strain, M. C.; Farkas, O.; Malick, D. K.; Rabuck, A. D.; Raghavachari, K.; Foresman, J. B.; Ortiz, J. V.; Cui, Q.; Baboul, A. G.; Clifford, S.;

Cioslowski, J.; Stefanov, B. B.; Liu, G.; Liashenko, A.; Piskorz, P.; Komaromi, I.; Martin, R. L.; Fox, D. J.; Keith, T.; Al-Laham, M. A.; Peng, C. Y.; Nanayakkara, A.; Challacombe, M.; Gill, P. M. W.; Johnson, B.; Chen, W.; Wong, M. W.; Gonzalez, C.; Pople, J. A. (2004): Gaussian 03, Revision E.01. Gaussian, Inc.: Wallingford, CT.

13. Khlifi, M.; Paillous, P.; Delpech, C.; Nishio, M.; Bruston, P.; Raulin, F. (1995): Absolute IR band intensities of diacetylene in the 250-4300 cm^{-1} region: implications for Titan's atmosphere. Journal of Molecular Spectroscopy 174, 116-122.
14. Seth-Paul, W. A. (1969): Classical and modern procedures for calculating PR separations of symmetrical and asymmetrical top molecules. Journal of Molecular Structure 3, 403-417.
15. van der Heijden, A. W. A. M.; Mens, A. J. M.; Bogerd, R.; Weckhuysen, B. M. (2008): Dehydrochlorination of intermediates in the production of vinyl chloride over lanthanium oxide-based catalysts. Catalysis Letters 122, 238-246.
16. Janzen, J.; Kraus, G. (1971): Specific surface area measurements of carbon black. Rubber Chemistry and Technology 44, 1287-1296.
17. Rodat, S.; Abanades, S.; Grivei, E.; Patrianakos, G.; Zygogianni, A.; Konstandopoulos, A. G.; Flamant, G. (2011): Characterization of carbon blacks produced by solar thermal dissociation of methane. Carbon 49, 3084-3091.
18. Fazekas P.; Bódis E.; Keszler A. M.; Czégény Zs.; Klébert Sz.; Károly Z.; Szépvölgyi J. (2013): Decomposition of chlorobenzene by thermal plasma processing. Plasma Chemistry and Plasma Processes 33, 765-778.
19. Aso, H.; Matsuoka, K.; Sharma, A.; Tomita, A. (2004): Structural analysis of PVC and PFA carbons prepared at 500-1000 °C based on elemental composition, XRD and HRTEM. Carbon 42, 2963-2973.

20. Ferrari, A. C.; Meyer, J. C.; Scardaci, V.; Casiraghi, C.; Lazzeri, M.; Mauri, F.; Piscanec, S.; Jiang, D.; Novoselov, K. S.; Roth, S.; Geim, A. K. (2006): Raman spectrum of graphene and graphene layers. Physical Review Letters 97, 187401.
21. Eiceman, G. A.; Hoffman, R. V.; Collins, M. C.; Long, Y-T.; Lu, M-Q. (1990): Chlorine substitution reactions of polycyclic aromatic hydrocarbons on fly ash from coal-fired power plants. Chemosphere 21, 35-41.
22. Molina, M. J.; Molina, L.T. (1984): The rate of the reaction of OH with HCl. International Journal of Chemical Kinetics 16, 1151-1160.
23. Fazekas P.; Keszler A. M.; Bódis E.; Drotár E.; Klébert Sz.; Károly Z.; Szépvölgyi J. (2015): Optical emission spectra analysis of thermal plasma treatment of poly(vinyl chloride). Open Chemistry 13, 549-556.
24. Jansson, S.; Fick, J.; Marklund, S. (2008): Formation and chlorination of polychlorinated naphthalenes (PCNs) in the post-combustion zone during MSW combustion. Chemosphere 72, 1138-1144.

List of Figure Captions:

Figure 1. Scheme of the plasma reactor.

Figure 2. Expanded deformational band (ν_5, perpendicular mode) of acetylene exhibiting P-, Q- and R-branches. The band origin (Q-branch) is at 729.7 cm^{-1}. Resolution: 0.5 cm^{-1}, pressure: 1 atm. Addition of N_2 gas in concentration of 100 ppm.

Figure 3. Expanded antisymmetric CH stretching (ν_3, parallel mode) of acetylene exhibiting P- and R-branches. The band origin is at 3287.3 cm^{-1}. Resolution: 0.5 cm^{-1}, pressure: 1 atm. Addition of N_2 gas in concentration of 1500 ppm.

Figure 4. Combination bands of CO_2 at 3612.5 and 3744.4 cm^{-1} (4b) are overlapping with the H_2O stretching bands near 3700 cm^{-1} (4a).

Figure 5. Spectra of overlapping deformational modes of C_2H_2 (ν_4) and CO_2 (ν_2).

Figure 6. Pyrolysis product of pure PVC with four basic components. (A: experimental spectrum, B: spectrum of C_2H_2, C: spectrum of HCl, D: spectrum of CO, E: spectrum of CO_2).

Figure 7. Extra overlapping band in the CH stretching region of acetylene. (a: measured spectrum, b: pure acetylene spectrum, c: difference of a-b).

Figure 8. Weak extra feature at the low frequency side of combination band of acetylene ($\nu_4+\nu_5$), with band origin at 1241.2 cm^{-1}.

Figure 9. Weak extra IR bands in the region of C≡C–H deformational modes. For assignation, see text.

Figure 10. Soot particle size and morphology obtained at (a) neutral conditions (PVC4) is shown. A significant increase of the particle size of particles was observed in the presence of hydrogen (PVC13).

Figure 11. Residual PVC grains in the solid soot product in (a) neutral condition (PVC4), but they are absent in oxidative conditions (b) (PVC9).

Figure 12a-e. Effect of the experimental conditions on the formation of PAHs: (a) plate power under neutral conditions, (b) feed rate under neutral conditions, (c) plate power in the presence of oxygen, (d) oxygen stoichiometric ratio, (e) hydrogen stoichiometric ratio.

Figure 13. Effect of the oxygen/PVC ratios on the concentrations of polychlorinated PAHs. In the absence of oxygen the concentrations of these molecules were below the detection limit.

List of Table Titles

Decomposition of Poly(vinyl chloride) in Inductively Coupled Radiofrequency Thermal Plasma

Péter Fazekas*, Zsuzsanna Czégény, János Mink, Eszter Bódis, Szilvia Klébert, Csaba Németh, Anna Mária Keszler, Zoltán Károly, János Szépvölgyi

Institute of Materials and Environmental Chemistry, Research Centre for Natural Sciences, Hungarian Academy of Sciences. Magyar tudósok körútja 2, 1115 Budapest, Hungary.

*corresponding author's e-mail address: fazekas.peter@ttk.mta.hu

Keywords: Poly(vinyl chloride), Polymer Waste, Thermal Decomposition, Radiofrequency Thermal Plasma, Fourier Transform Infrared Spectroscopy, Gas Chromatography/Mass Spectrometry

Abstract

Decomposition of poly(vinyl chloride) (PVC) was studied in inductively coupled radiofrequency thermal plasma in neutral, oxidative and reductive conditions. The exhaust gases were analysed by Fourier transform infrared spectroscopy (FT-IR), and their main components were identified as CO, CO_2, C_2H_2, H_2O and HCl. The weaker bands in the infrared spectra were assigned by density function theory calculations and P-R separation method. The extent of PVC decomposition was calculated from the amount of solid soot, which was also studied by transmission electron microscopy (TEM) for morphology and composition. Organic compounds adsorbed on the surface of the soot were extracted by toluene and analysed by gas chromatography mass spectrometry (GC/MS). The extracts

comprised of various polycyclic aromatic hydrocarbons (PAHs) and their methylated and chlorinated derivatives. Their amount was greatly affected by the experimental conditions. The presence of oxygen decreased the formation of PAHs, while it increased the formation of polychlorinated PAH compounds. In the presence of hydrogen PAH formation was observed. However, dioxin or furan derivatives were not detected in the decomposition products.

1. Introduction

Poly(vinyl chloride) (PVC) is one of the most common polymeric material with a production of 38.5 million tons in 2013, which accounted for 12 % of the total plastic production worldwide. The demand for PVC is increasing, therefore production is forecasted to rise by 3.2 % per year by 2021 [1], due to the broad usage of PVC in many areas of everyday life, such as the building industry (doors, window frames, pipes, cables), computers (keyboards, cases, various peripheries), medical devices (blood and plasma bags), clothing (raincoats, imitation leathers, rubber boots), food packaging (containers, bottles) and in the administrative sector (credit cards, identity cards) [2]. In usual environmental conditions PVC is a stable material and is not prone to decomposition reactions. Only its grain size decreases due to physical weathering. After its lifespan the deposition of PVC in landfills requires more and more space, which means increasing environmental impacts and expenses. Therefore, development of reliable recycling or decomposition methods is an urgent necessity. Although several technologies have been proposed for recycling, they have not reached a commercially feasible solution yet [3]. Thermal degradation of PVC via conventional high temperature decomposition such as pyrolysis or cracking results in toxic by-products, which are stable and also present hazards both on human health and the environment. Significant amounts of

benzene and toluene are being formed on decomposition of PVC due to ring closing reactions taking place after the elimination of HCl from the polymer chain [4]. This can be modified by metals, metal oxides or other polymers [5-6]. In addition, the presence of PVC has remarkable impact on the decomposition of numerous plastics [6]. Thermal decomposition of PVC along with lignocellulose biomass materials results in significant formation of chloromethane [7]. During incineration of PVC formation of different types of dioxins and furans were also reported [8].

The inductively coupled thermal plasmas (IC-TPs), which are characterized by high temperature and energy density, contain photons, ground-state and excited atoms, ions and molecules. Due to their special properties IC-TPs offer an environmental benign solution for the destruction of organic materials and polymers, too. The extremely high temperature (8000–12000 K) and strong UV radiation facilitate decomposition and induce a large number of reactive species. The high quenching rate of gases (~10^6 K s^{-1}) is advantageous to avoid the recombination of radicals into large, stable molecules, like dioxins. Therefore, this technique has been increasingly applied in waste treatment, for example in the decomposition of chlorine-free polymers [9] and halogenated organic molecules [10-11], as well.

In this paper we report on the decomposition of PVC in IC-TP plasma in neutral, oxidative and reductive conditions. The decomposition process was characterized by the analysis of all gaseous, liquid and solid products. On the basis of experimental results, the most favourable conditions of PVC decomposition were determined in the particular system.

2. Materials and methods

In this study PVC powder, as a model, was applied free of additives, and was supplied by BorsodChem Co. (Hungary). The number average molar mass (M_n) was 28150 g mole^{-1}, its mass average molar mass (M_w) was 89660 g mole^{-1} and had an average particle size of 150 μm.

The experimental set-up consisted of an RF inductively coupled plasma torch (TEKNA PL-35) connected to a high frequency (4–5 MHz) LEPEL generator, a reactor, a cyclone, a filter unit and a vacuum pump. The PVC powder was fed axially into the hottest zone of the plasma column by a PRAXAIR powder feeder and an atomizer nozzle of 2.16 mm inner diameter. For the atomization Ar flow (99.996 % purity, Messer Hungarogáz Ltd.) of 9.4 dm^3 min^{-1} was used. The plasma torch was also operated with Ar central gas and sheath gas with flow rates of 15.5 and 35.5 dm^3 min^{-1}, respectively. In certain runs O_2 (99.5 %, Messer Hungarogáz Ltd.) or H_2 (99.98 %, Linde Gáz Magyarország Ltd.) was added into the sheath gas in different concentrations. The double-wall, water cooled cylindrical reactor shown in Figure 1, was made of stainless steel with the inner diameter of 19.7 cm and length of 121.6 cm. To determine the optimal conditions of decomposition, the following plasma parameters were changed in particular tests: (1) feeding rate of PVC (50–150 g h^{-1}), (2) oxygen and hydrogen concentration (in various stoichiometric ratios) and (3) plate power (15–25 kW). The experimental conditions are listed in Table 1. Stoichiometric ratios were calculated by assuming a complete oxidation (into CO_2, H_2O and HCl) and reduction (into CH_4 and HCl) of PVC, respectively. Tests designated as PVC1 and PVC2 stood for the blank samples of GC/MS measurements.

The exhaust gases were collected in a standard through-flow gas cell of 10 cm length equipped with KBr windows. Middle-infrared spectra (350-4000 cm^{-1}) were recorded by a Varian FTS-7000 high resolution (0.08 cm^{-1}) Fourier transform infrared spectrometer (FT-IR). The spectrometer had a dynamically aligned interferometer, a Peltier-thermostated

deutero triglycine sulphate (DTGS) detector and a high intensity ceramic source. 16 scans were accumulated from every sample with the resolution of 0.5 cm^{-1}. Quantitative analysis was done by the integration method using the Quasoft database, which contains the spectra of 250 small sized atmospheric contaminants with known concentration.

Density functional theory (DFT) calculations were used to define the fundamental frequencies, the IR and Raman intensities and the moments of inertia of expected acetylene derivatives. These calculations were carried out by the Gaussian 03 code. [12]

The solid soot was collected from the wall of the plasma reactor. Morphology of soot particles was characterized by transmission electron microscopy (TEM, Morgagni 268D). The specific surface area was measured by N_2 adsorption at 77 K using a 11-point BET method (Quantachrome, Autosorb-1).

Organic compounds adsorbed on the surface of the soot were ultrasonically extracted by toluene (Merck, HPLC grade purity). 10 mg soot was treated in 2 cm^3 toluene for 60 minutes. The extracts were analysed by GC/MS (Agilent Technologies Inc. 6890 GC/5973 MSD) using Agilent DB-1701 capillary column (30 m length, 0.25 mm inner diameter, 0.25 μm film thickness). 1 μl sample was injected to the column in splitless injection mode. Temperature of the GC injector was kept at 300 °C. The GC oven was hold at 50 °C for 1 min, and then increased to 280 °C at a rate of 10 °C min^{-1}. The mass spectrometer was operated at 70 eV in the electron impact ionisation mode. The mass detection ranged from 14 to 500 Da.

3. Results and Discussion

3.1 Analysis of the exhaust gases

3.1.1 Qualitative analysis

Decomposition of three PVC samples was studied by FT-IR; (1) pure PVC in Ar (PVC4), (2) pure PVC in O_2 (PVC9) and (3) pure PVC in H_2 (PVC13). The major components in the plasma gases were CO_2, CO, H_2O, C_2H_2 and HCl. All rotational-vibrational spectra of the small molecules are very different and very characteristic. The presence of oxygen containing species in neutral conditions can be explained by presence of oxygen traces of about 50 ppm in the Ar carrier, plasma and sheath gases.

Three well defined infrared bands of acetylene were observed at 729.7 (ν_5), 1326.4 ($\nu_4+\nu_5$) and 3287.3 (ν_3) cm^{-1} frequencies. The ν_5 refers to deformational (linear bending) mode of HCCH (perpendicular band) which exhibits P-, Q- and R-branches. The origin of the ν_5 band is at the maximum position of the Q-branch, which is illustrated in Figure 2. In contrast, the antisymmetric CH stretching (ν_3) is a so called parallel band exhibiting well separated P- and R-branches. In this case the band origin is in the middle of P- and R-branches, at 3287.3 cm^{-1} (Figure 3). Except the above discussed two fundamental modes (ν_3 and ν_5) there is another IR-active band exhibiting fine structure of parallel mode, which is a combination band of ν_4 and ν_5 fundamentals and detected at 1326.4 cm^{-1}. The ν_4 mode is only Raman active, observed at 611.8 cm^{-1} and its combination with ν_5 gives 1341.5 cm^{-1} which moves down to 1326.4 cm^{-1} due to an-harmonic vibrations.

Four well defined bands can be obtained in the IR spectrum of CO_2, at 667.6 (ν_2), 2348.7 (ν_3), 3616.2 ($2\nu_2+\nu_3$) and 3714.4 cm^{-1} ($\nu_1+\nu_3$). The bending mode (ν_2) exhibit P-, Q- and R-branches as perpendicular vibration. The antisymmetric CO_2 stretching (ν_3) has only P- and R-branches characteristic for bands of parallel vibrations (the induced dipole moment is parallel with the molecular axis). The two combination bands are also parallel modes with P- and R-branches.

The diatomic gas species (CO and HCl) both have one parallel fundamental mode with P- and R-branches.

The above described linear (C_2H_2, CO_2) and diatomic (CO, HCl) molecules gave rather similar band structures with P-, Q- and R-branches or with P- and R-branches. All these molecules have only one moment of inertia. But the H_2O as an asymmetric rotor has three different moment of inertia consequently exhibiting very complicated rotational fine structure, and even not easy to obtain the band origin. The three fundamentals obtained by theoretical analysis are at 1594.6 (ν_2), 3656.7 (ν_1) and 3755.8 (ν_3) cm^{-1} and a weak overtone is at 3154.4 ($2\nu_2$) cm^{-1}.

3.1.2 Quantitative analysis

Due to the rotational fine structure even the gas spectra of small molecules spread a broad range. This can lead to overlapping of bands of different molecules. Such a case is shown in Figure 4, where overtones of CO_2 overlap with OH stretching bands of H_2O. Similar situation was observed between deformation modes of C_2H_2 (ν_5) and CO_2 (ν_2) near 700 cm^{-1} (Figure 5). With careful spectral subtractions the effect of overlapping can be eliminated before concentration determination. Another problem is that the quantity of CO_2 and H_2O gases can always be determined with difficulties due to their permanent but variable presence in the atmosphere.

In Figure 6 the spectra of the pyrolysis products from PVC are shown. The library spectra of the main components, i.e. C_2H_2, HCl, CO and CO_2 were used for quantitative analysis. The results obtained by method of integration of experimental intensities are summarised in Table 2. Degradation of PVC in Ar produced large amount of hydrochloric acid (104.2 μmole dm^{-3}) and acetylene (38.6 μmole dm^{-3}).

In presence of hydrogen the decomposition results in smaller amount of HCl (30.6 μmole dm^{-3}). No CO formation was detected. However, presence of hydrogen has no effect on C_2H_2 formation of as its concentration does not change. The higher amount of CO_2 and the large concentration of H_2O may be attributed to the oxygen contamination of commercial hydrogen.

The decomposition process was more "complete" in the presence of oxygen, leading to CO_2, HCl and H_2O as main products.

3.1.3 Minor products

A more detailed analysis of IR spectra in Figure 6 refers to several additional weak bands. An extra overlapping band can be seen in the CH stretching region of acetylene in the high frequency side (Figure 7). The experimental spectrum 8a in Figure 7 showing the decomposition products of pure PVC contains not resolved extra bands at 3340 (R), 3332 (band origin) and 3323 (P) cm^{-1} (Figure 7 (8c)), which was obtained by subtraction of the spectrum of pure acetylene (Figure 7 (8b)).

Weak P- and R-branches were observed at 1248 and 1233 cm^{-1} with band origin at 1241.2 cm^{-1}, near the $\nu_4+\nu_5$ combination band (1326.9 cm^{-1}) of acetylene (Figure 8).

The strongest band in the region of C≡C–H deformation of acetylenes was observed at 628 cm^{-1} (Figure 9).

The above discussed three extra bands nicely correlate with the experimental IR data of di-acetylene (butadiene). The band origins at 3332, 1241 and 628 cm^{-1} [13] well correlate with our observations at 3332, 1241.2 and 628 cm^{-1} obtained in the sample of decomposition products of PVC. Our scaled DFT calculation gave 3341, 1294 and 628 cm^{-1}. The infrared active modes of di-acetylene are summarised in Table 3. The agreement of the wavenumbers

in the table is very good, but big discrepancies were observed between the experimental and the calculated band intensities.

The above assignments can be supported by the P-R band separation of di-acetylene. This method is used when bands of several molecules are very close to each other, therefore the assignation of the bands based on the spectral position is not possible. The well-known formula of band separation is given by Equation 1., as follows:

$$\Delta\nu_{\text{P-R}} = \left(\frac{8k}{hc}BT\right)^{0.5} = 2.3583(BT)^{0.5} \quad (1)$$

where $\Delta\nu_{\text{P-R}}$ is the value of the P-R separation, T is the absolute temperature, B is the rotational constant in cm^{-1} unit, k is the Boltzmann constant, h is the Planck constant and c is the velocity of light in vacuum [14]. In case of diacetylene B = 0.1326 cm^{-1} which gives $\Delta\nu_{\text{P-R}}$ = 14.9 cm^{-1}. In Table 3. the ν_4 band has 17 cm^{-1} and the $\nu_6+\nu_8$ combination band has 15.6 cm^{-1} P-R separations, which are agreed well with the theoretically predicted value. On the other hand, the calculated band separation of triacetylene (C_6H_2) is 8.5 cm^{-1} which is far from our experimental observations.

According to DFT calculation of polyacetylenes the IR active C≡C–H linear bending mode is expected at 729, 628, 617 and 616 cm^{-1} for C_2H_2, C_4H_2, C_6H_2 and C_8H_2, respectively. The weak bands in Figure 9 at 621.4 and 615.6 cm^{-1} may be assigned to trace amount of triacetylene and tetraacetylene, respectively. Unfortunately, it is difficult to assign the other weak bands in this region at 635, 634, 625 and 613 cm^{-1}.

The monochloroacetylene has a strong band at 607 cm^{-1}, which can be assigned to the lowest band at 613 cm^{-1}, but it also has another strong band at 2110 cm^{-1} which was not detected in our experiments [15].

3.2 Solid products analysis

In each test a black, solid soot, was collected from the reactor wall. Its yield from the decomposition was calculated according to Equation 2.:

$$\text{Soot yield} = \frac{\text{Amount of soot formed } (\text{g h}^{-1})}{\text{Carbon content of PVC fed } (\text{g h}^{-1})} \qquad (2)$$

Soot yields calculated by Eq. (2) are shown in Table 4. In Ar plasma the increase of plate power from 15 to 20 kW (PVC3 and PVC4) did not change the soot yield. However, at plate power of 25 kW (PVC5) the soot yield decreased by 8.6 % as compared to PVC4, which represents a relative decrease of about 25 %. The change in feed rate in the 50-150 g h^{-1} range did not show any effect on the soot yield. In the presence of oxygen increase of the plate power resulted in lower soot yield, most significantly at 25 kW (PVC8-10). Both sets of experiments, performed in Ar and in Ar+O_2, show that higher plate power leads to greater degree of gasification. Test with 1:2 oxygen/PVC stoichiometric ratio (PVC11) actually did not differ from that in neutral conditions (PVC4). In reductive conditions, applying Ar+H_2 plasma, soot formation decreased significantly as compared to neutral ones.

Specific surface area (SSA) of selected soot samples (Table 5.) varied in the range of 60 and 100 m^2 g^{-1}, which is typical for carbon blacks [16-17]. At the highest feed rate (PVC7) the low SSA value implies larger soot particles.

TEM micrographs of the soot samples depicted in Figure 10, show typical plate like particles with their size varied between 20-30 nm. Interestingly both in reductive and oxidative conditions, it increased to 40-50 nm in Ar+H_2 and to 60-80 nm in Ar+O_2. These values are in good agreement with our former results [18]. However, in neutral conditions the soot also contained particles with typical size of 200-1000 nm, which were identified as grains

of unreacted PVC (Figure 11). Therefore, for complete decomposition of PVC, oxidative or reductive conditions are required in the particular experimental system. In oxidative conditions the oxygen attacks the polymer chain, while hydrogen improves the heat transfer between the plasma flame and PVC particles due to its higher heat conductivity as compared to argon.

Based on the results of Japanese researchers [19] we also investigated possible the formation of graphene in the applied conditions. No specific G or 2D peaks of graphene at 1580 and 2700 cm^{-1} [20], respectively were detected in the Raman spectra of sample from Runs PVC4, 7, 9 and 14.

3.3 Analysis of extracts from the soot

3.3.1 Qualitative analysis of organic compounds extracted from the soot

The organic compounds adsorbed on the surface of the soot were extracted by toluene. The extracts were analysed by GC/MS, and the identified compounds are listed in Table 6.

With the exception of the linear hexachlorobutadiene all identified compounds were aromatic or polyaromatic hydrocarbons (PAH) and their methylated or chlorinated derivatives. Diacetylene and triacetylene, as probable building blocks of PAHs before the ring closing reactions, were detected in the gas phase by FT-IR. We did not detect any dioxins or furans, the only oxygen containing molecule was benzaldehyde.

In the presence of hydrogen we could observe only a slight change in the composition of the PAHs: the concentration of dimethylbiphenyl decreased below the detection limit. By contrast, the oxidative atmosphere had huge impact on the formation of by-products. Six compounds could not be detected, amongst them indenophenanthrene and benzoperylene

were the largest non-chlorinated molecules in the extracts, three (dimethylphenanthrene, phenylmethylnaphthalene, methylchrysene) were methylated PAH molecule and terphenyl was a three ring PAH. The oxygen reacts with the C_2 and CH radicals, which are the building blocks of polycyclic hydrocarbons. By decreasing the concentration of these radicals, the formation of larger molecules is less probable. Another effect of the oxygen was the appearance of polychlorinated PAHs, such as hexachlorobenzene or octochloronaphthalene. Several monochlorinated compounds have been identified under neutral conditions (chloronaphthalene, chloroanthracene, chloropyrene), which is in agreement with the literature [21], but higher degree of chlorination occurred only in oxidative conditions. We detected mainly the polychlorinated derivatives of benzene and naphthalene, even their perchlorinated variants. Hexachlorobutadiene was also detected, which is a fully chlorinated linear molecule. In view of our previous work [18], presence of such type of molecules was unexpected, but other papers confirm the possibility of its formation from chlorinated linear hydrocarbons in IC-TP plasmas [11]. This enhanced chlorination process can be attributed to the reaction between HCl and OH (Equation 3):

$$HCl + OH = H_2O + Cl \quad (3)$$

which is a well-established reaction in stratospheric chemistry [22]. The presence of the two precursors is known from the FT-IR data and our former optical emission measurements as well [23]. The newly formed chlorine radical attacks the aromatic rings and substitutes a hydrogen atom. Due to the large number of chlorine radicals this process leads to polychlorination [24].

3.3.2 Quantitative analysis of organic compounds extracted from the soot

Five different sets in the experimental conditions were investigated: the effect of plate power (1) and feed rate (2) under neutral condition, the effect of plate power (3) and stoichiometric ratio (4) in oxidative atmosphere and the effect of stoichiometric ratio (5) in the presence of hydrogen. The extracts consisted mostly of three and four ring molecules in each condition.

The influence of plate power under neutral condition showed controversial impact. The increase from 15 to 20 kW resulted in a significant decrease in the concentration of the PAH compounds in every ring number category, however at 25 kW the concentrations started to rise in small extent (Figure 12a).

Higher feed rates resulted in higher PAH concentrations (Figure 12b). The higher amount of material in the plasma flame reduced the specific energy and that lower amount was not sufficient to prevent the recombination of the larger number of fragments into larger molecules.

The influence of plate power on the concentrations of PAHs in oxidative atmosphere was similar as it was found in the absence of oxygen (Figure 12c). Increasing it from 15 to 20 kW resulted a slight decrease in concentrations, but in a much lower degree than in case of neutral atmosphere. At 25 kW the two ring molecules decreased, but the concentrations of the three and for ring compound increased higher than at 15 kW. However, the effect of oxygen was significant, the PAH concentrations were one order of magnitude lower than in neutral environment. Furthermore, as mentioned above, the largest, six ring molecules disappeared completely, while one ring compounds were detected only in oxidative conditions.

Increasing the oxygen content to the 1:1 stoichiometric ratio resulted an obvious drop in the concentration of the PAH molecules (Figure 12d). At 1:2 ratio the soot yield was not different from the neutral condition (Table 4.) which showed that the oxygen reacted with the

HCl instead of the carbon. The appearance of the polychlorinated compounds supports this theory (Figure 13). At higher oxygen rates their concentrations dropped because the increased amount of oxygen was able to react with the building aromatic rings.

The reductive environment was detrimental to the decomposition process. The presence of hydrogen increased the amount of PAH compounds at every stoichiometric rate (Figure 12e). The hydrogen did not react with the small carbon molecules and fragments, like C_2, and CH, to form stable gaseous hydrocarbons, instead assisted in the formation of largerthe enlargement and enrichment of the PAHs.

4. Conclusions

In this study PVC powder was used as a model compound to reveal the decomposition processes of such type of halogenated polymers in inductively coupled radiofrequency thermal plasma. TEM analysis of the solid products revealed that the decomposition of PVC was not complete in Ar plasma, therefore addition of auxiliary gases, such as oxygen or hydrogen is required.

The exhaust gases from the plasma reactor mainly consist of acetylene, hydrogen chloride, carbon dioxide, carbon monoxide and water vapour. Different polyacetylenes, the building blocks of the PAHs were also detected in the gaseous products.

Formation of a large number of different polyaromatic hydrocarbons could be detected by the analysis of soot. As they have adverse effect on the environment and human health so their formation should be minimized. Their analysis revealed some important tendencies, which should be taken into account in designing the decomposition process. Increased feed rate leads to higher PAH formation. Therefore, the emission thresholds of PVC

decomposition must be monitored closely. According to our findings, higher plate power does not result in more complete decomposition. Thus, it is not necessary to operate the plasma generator with maximum plate power in particular conditions. Presence of oxygen hinders formation of PAHs. On the other hand, in the absence of oxygen no polychlorinated PAHs are formed. Hydrogen increases formation of PAHs, especially those with higher ring numbers, therefore its presence is detrimental.

Acknowledgement: This work has been supported by the National Development Agency of Hungary (Grant No. KTIA_AIK_12-1-2012-0004).

References

1. Yu, J.; Sun, L.; Ma, C.; Qiao, Y.; Yao, H. (2016): Thermal degradation of PVC: A review. Waste Management 48, 300-314.
2. Moulay, S. (2010): Chemical modification of poly(vinyl chloride)-Still on the run. Progress in Polymer Science 35, 303-331.
3. Shadat-Sojai, M.; Bekhschandeh, G.-R. (2011): Recycling of PVC wastes. Polymer Degradation and Stability 96, 404-415.
4. Miranda, R.; Yang, J.; Roy, C.; Vasile, C. (1999): Vacuum Pyrolysis of PVC I. Kinetic study. Polymer Degradation and Stability 64, 127-144.
5. Blazsó M.; Jakab E. (1999): Effect of metals, metal oxides and carboxylates on the thermal decomposition processes of poly (vinyl chloride). Journal of Analytical and Applied Pyrolysis 49, 125-143.
6. Czégény Zs.; Jakab E.; Blazsó M. (2002): Thermal decomposition of polymer mixtures containing poly (vinyl chloride). Macromolecular Materials and Engineering 287, 277-284.

7. Czégény Zs.; Jakab E.; Bozi J.; Blazsó M. (2015): Formation of chloromethane from lignocellulosic materials in the presence of PVC. Journal of Analytical and Applied Pyrolysis 113, 123-132.
8. Christmann, W.; Kasiske, D.; Klöppel, K. D.; Partscht, H.; Rotard, W. (1989): Combustion of polyvinylchloride- an important source for the formation of PCDD/PCDF. Chemosphere 19, 387-392.
9. Gudetti, R. R.; Knight, R.; Grossmann, E. D. (2000): Depolymerization of polyethylene using induction-coupled plasma technology. Plasma Chemistry and Plasma Processing 20, 37-64.
10. Főglein K. A.; Szépvölgyi J.; Szabó T. P.; Mészáros E.; Jakab E.; Babievskaya, I. Z.; Mohai I.; Károly Z. (2005): Comparative study on decomposition of $CFCl_3$ in thermal and cold plasma. Plasma Chemistry and Plasma Processing 25, 275-288.
11. Főglein K. A.; Szabó P. T.; Babievskaya, I. Z.; Szépvölgyi J. (2005): Comparative study on the decomposition of chloroform in thermal and cold plasma. Plasma Chemistry and Plasma Processing 25, 289-301.
12. Frisch, M. J.; Trucks, G. W.; Schlegel, H. B.; Scuseria, G. E.; Robb, M. A.; Cheeseman, J. R.; Montgomery, Jr., J. A.; Vreven, T.; Kudin, K. N.; Burant, J. C.; Millam, J. M.; Iyengar, S. S.; Tomasi, J.; Barone, V.; Mennucci, B.; Cossi, M.; Scalmani, G.; Rega, N.; Petersson, G. A.; Nakatsuji, H.; Hada, M.; Ehara, M.; Toyota, K.; Fukuda, R.; Hasegawa, J.; Ishida, M.; Nakajima, T.; Honda, Y.; Kitao, O.; Nakai, H.; Klene, M.; Li, X.; Knox, J. E.; Hratchian, H. P.; Cross, J. B.; Bakken, V.; Adamo, C.; Jaramillo, J.; Gomperts, R.; Stratmann, R. E.; Yazyev, O.; Austin, A. J.; Cammi, R.; Pomelli, C.; Ochterski, J. W.; Ayala, P. Y.; Morokuma, K.; Voth, G. A.; Salvador, P.; Dannenberg, J. J.; Zakrzewski, V. G.; Dapprich, S.; Daniels, A. D.; Strain, M. C.; Farkas, O.; Malick, D. K.; Rabuck, A. D.; Raghavachari, K.; Foresman, J. B.; Ortiz, J. V.; Cui, Q.; Baboul, A. G.; Clifford, S.;

Cioslowski, J.; Stefanov, B. B.; Liu, G.; Liashenko, A.; Piskorz, P.; Komaromi, I.; Martin, R. L.; Fox, D. J.; Keith, T.; Al-Laham, M. A.; Peng, C. Y.; Nanayakkara, A.; Challacombe, M.; Gill, P. M. W.; Johnson, B.; Chen, W.; Wong, M. W.; Gonzalez, C.; Pople, J. A. (2004): Gaussian 03, Revision E.01. Gaussian, Inc.: Wallingford, CT.

13. Khlifi, M.; Paillous, P.; Delpech, C.; Nishio, M.; Bruston, P.; Raulin, F. (1995): Absolute IR band intensities of diacetylene in the 250-4300 cm^{-1} region: implications for Titan's atmosphere. Journal of Molecular Spectroscopy 174, 116-122.
14. Seth-Paul, W. A. (1969): Classical and modern procedures for calculating PR separations of symmetrical and asymmetrical top molecules. Journal of Molecular Structure 3, 403-417.
15. van der Heijden, A. W. A. M.; Mens, A. J. M.; Bogerd, R.; Weckhuysen, B. M. (2008): Dehydrochlorination of intermediates in the production of vinyl chloride over lanthanium oxide-based catalysts. Catalysis Letters 122, 238-246.
16. Janzen, J.; Kraus, G. (1971): Specific surface area measurements of carbon black. Rubber Chemistry and Technology 44, 1287-1296.
17. Rodat, S.; Abanades, S.; Grivei, E.; Patrianakos, G.; Zygogianni, A.; Konstandopoulos, A. G.; Flamant, G. (2011): Characterization of carbon blacks produced by solar thermal dissociation of methane. Carbon 49, 3084-3091.
18. Fazekas P.; Bódis E.; Keszler A. M.; Czégény Zs.; Klébert Sz.; Károly Z.; Szépvölgyi J. (2013): Decomposition of chlorobenzene by thermal plasma processing. Plasma Chemistry and Plasma Processes 33, 765-778.
19. Aso, H.; Matsuoka, K.; Sharma, A.; Tomita, A. (2004): Structural analysis of PVC and PFA carbons prepared at 500-1000 °C based on elemental composition, XRD and HRTEM. Carbon 42, 2963-2973.

20. Ferrari, A. C.; Meyer, J. C.; Scardaci, V.; Casiraghi, C.; Lazzeri, M.; Mauri, F.; Piscanec, S.; Jiang, D.; Novoselov, K. S.; Roth, S.; Geim, A. K. (2006): Raman spectrum of graphene and graphene layers. Physical Review Letters 97, 187401.
21. Eiceman, G. A.; Hoffman, R. V.; Collins, M. C.; Long, Y-T.; Lu, M-Q. (1990): Chlorine substitution reactions of polycyclic aromatic hydrocarbons on fly ash from coal-fired power plants. Chemosphere 21, 35-41.
22. Molina, M. J.; Molina, L.T. (1984): The rate of the reaction of OH with HCl. International Journal of Chemical Kinetics 16, 1151-1160.
23. Fazekas P.; Keszler A. M.; Bódis E.; Drotár E.; Klébert Sz.; Károly Z.; Szépvölgyi J. (2015): Optical emission spectra analysis of thermal plasma treatment of poly(vinyl chloride). Open Chemistry 13, 549-556.
24. Jansson, S.; Fick, J.; Marklund, S. (2008): Formation and chlorination of polychlorinated naphthalenes (PCNs) in the post-combustion zone during MSW combustion. Chemosphere 72, 1138-1144.

List of Figure Captions:

Figure 1. Scheme of the plasma reactor.

Figure 2. Expanded deformational band (ν_5, perpendicular mode) of acetylene exhibiting P-, Q- and R-branches. The band origin (Q-branch) is at 729.7 cm^{-1}. Resolution: 0.5 cm^{-1}, pressure: 1 atm. Addition of N_2 gas in concentration of 100 ppm.

Figure 3. Expanded antisymmetric CH stretching (ν_3, parallel mode) of acetylene exhibiting P- and R-branches. The band origin is at 3287.3 cm^{-1}. Resolution: 0.5 cm^{-1}, pressure: 1 atm. Addition of N_2 gas in concentration of 1500 ppm.

Figure 4. Combination bands of CO_2 at 3612.5 and 3744.4 cm^{-1} (4b) are overlapping with the H_2O stretching bands near 3700 cm^{-1} (4a).

Figure 5. Spectra of overlapping deformational modes of C_2H_2 (ν_4) and CO_2 (ν_2).

Figure 6. Pyrolysis product of pure PVC with four basic components. (A: experimental spectrum, B: spectrum of C_2H_2, C: spectrum of HCl, D: spectrum of CO, E: spectrum of CO_2).

Figure 7. Extra overlapping band in the CH stretching region of acetylene. (a: measured spectrum, b: pure acetylene spectrum, c: difference of a-b).

Figure 8. Weak extra feature at the low frequency side of combination band of acetylene ($\nu_4+\nu_5$), with band origin at 1241.2 cm^{-1}.

Figure 9. Weak extra IR bands in the region of C≡C–H deformational modes. For assignation, see text.

Figure 10. Soot particle size and morphology obtained at (a) neutral conditions (PVC4) is shown. A significant increase of the particle size of particles was observed in the presence of hydrogen (PVC13).

Figure 11. Residual PVC grains in the solid soot product in (a) neutral condition (PVC4), but they are absent in oxidative conditions (b) (PVC9).

Figure 12a-e. Effect of the experimental conditions on the formation of PAHs: (a) plate power under neutral conditions, (b) feed rate under neutral conditions, (c) plate power in the presence of oxygen, (d) oxygen stoichiometric ratio, (e) hydrogen stoichiometric ratio.

Figure 13. Effect of the oxygen/PVC ratios on the concentrations of polychlorinated PAHs. In the absence of oxygen the concentrations of these molecules were below the detection limit.

List of Table Titles

Table

Table 1. The experimental conditions

Run	Plate power (kW)	Feed rate (g h^{-1})	Auxiliary gases (stoichiometric ratio)
PVC3	15	50	–
PVC4	20	50	–
PVC5	25	50	–
PVC6	20	100	–
PVC7	20	150	–
PVC8	15	50	1 O_2
PVC9	20	50	1 O_2
PVC10	25	50	1 O_2
PVC11	20	50	0,5 O_2
PVC12	20	50	0,5 H_2
PVC13	20	50	1 H_2

Table 2. Concentration of the main gaseous components from PVC decomposition

Run	Measured component	Band origin frequency (cm^{-1})	Concentration ($\mu mole\ dm^{-3}$)
PVC4 (pure PVC)	CO_2	2348.7	1.0
	CO	2143.6	9.5
	HCl	2885.6	104.2
	C_2H_2	729.7, 1326.4, 3287.3	38.6
PVC9 (PVC+O_2)	CO_2	2348.7	169.4
	HCl	2885.6	81.0
	H_2O	1594.6	379.3
PVC13 (PVC+H_2)	CO_2	2348.7	5.0
	HCl	2885.6	30.6
	C_2H_2	729.7	38.8
	H_2O	1594.6	202.0

Table 3. Characteristic IR bands of diacetylene

Literature [13]		**Experiment**		**DFT calculation**	
Wavenumber (cm^{-1})	Absolute intensity	Wavenumber (cm^{-1})	Absolute intensity	Wavenumber (cm^{-1})	Absolute intensity
3340 R 3332 ν_4 3324 P	488	3340 R 3332 ν_0 3323 P	490[a] (0.646)[b]	3341	490[a] (189)[c]
1248 R 1241 $\nu_6+\nu_8$ 1234 P	171	1248.6 R 1241.2 ν_0 1233 P	155 (0.205)[b]	1294	–
628 Q, ν8	437	628 Q, ν_0	254[a] (0.336)[b,*]	628	228[a] (88)[c]

a: scaled values of experimental data are in atm^{-1} cm^{-2} units

b: arbitrary integrated band intensities

c: DFT calculated intensities are in $km \cdot mole^{-1}$ units

*: overlapping with other bands

Table 4. Soot yields of PVC decomposition

Run	Soot yield (%)
PVC3	39,65
PVC4	40,23
PVC5	31,59
PVC6	38,11
PVC7	38,15
PVC8	34,52
PVC9	31,66
PVC10	18,52
PVC11	38,90
PVC12	27,26
PVC13	20,25

Table 5. Specific Surface Area (SSA) of selected soot samples

Run	SSA (m^2 g^{-1})
PVC4	106
PVC7	44
PVC9	88
PVC13	70

Table 6. Compounds identified in the toluene extracts

No.	Compounds	Formula	m/z	Presence (neutral, reductive)	Presence (oxidative)
1.	Benzaldehyde	C_7H_6O	106	–	+
2.	Naphthalene	$C_{10}H_8$	128	+	+
3.	Methylnaphthalene	$C_{11}H_{10}$	142	+	+
4.	Pentylbenzene	$C_{11}H_{16}$	148	+	+
5.	Biphenylene	$C_{12}H_8$	152	+	+
6.	Biphenyl	$C_{12}H_{10}$	154	+	+
7.	Chloronaphthalene	$C_{10}H_7Cl$	162	+	+
8.	Fluorene	$C_{13}H_{10}$	166	+	+
9.	Phanenthrene/anthracene	$C_{14}H_{10}$	178	+	+
10.	Diphenylmethylene/methylfluorene	$C_{14}H_{12}$	180	+	+
11.	Dimethylbiphenyl	$C_{14}H_{14}$	182	+ *	+
12.	Cyclopentaphenanthrene	$C_{15}H_{10}$	190	+	+
13.	Methylphenanthrene	$C_{15}H_{12}$	192	+	+
14.	Dichloronaphthalene	$C_{10}H_6Cl_2$	196	–	+
15.	Pyrene/Fluoranthene	$C_{16}H_{10}$	202	+	+
16.	Phenylnaphthalene	$C_{16}H_{12}$	204	+	+
17.	Dimethylphenanthrene	$C_{16}H_{14}$	206	+	–
18.	Chloroanthracene	$C_{14}H_9Cl$	212	+	+
19.	Methylpyrene	$C_{17}H_{12}$	216	+	+
20.	Tetrachlorobenzene	$C_6H_2Cl_4$	216	–	+
21.	Phenylmethylnaphthalene	$C_{17}H_{14}$	218	+	–
22.	Cyclopentapyrene	$C_{18}H_{10}$	226	+	+
23.	Triphenylene/chrysene	$C_{18}H_{12}$	228	+	+
24.	Terphenyl	$C_{18}H_{14}$	230	+	–
25.	Trichloronaphthalene	$C_{10}H_5Cl_3$	230	–	+
26.	Chloropyrene	$C_{16}H_9Cl$	236	+	+
27.	Methylchrysene	$C_{19}H_{14}$	242	+	–
28.	Dichloroanthracene	$C_{14}H_8Cl_2$	246	–	+
29.	Pentachlorobenzene	C_6HC_{l5}	250	–	+
30.	Benzapyrene	$C_{20}H_{12}$	252	+	+
31.	Binaphthalene	$C_{20}H_{14}$	254	+	+
32.	Hexachlorobutadiene	C_4Cl_6	258	–	+
33.	Indenophenanthrene	$C_{21}H_{14}$	266	+	–
34.	Tetrachloronaphthalene	$C_{10}H_4Cl_4$	266	–	+
35.	Benzoperylene	$C_{22}H_{12}$	276	+	–
36.	Hexachlorobenzene	C_6Cl_6	284	–	+
37.	Octochloronaphthalene	$C_{10}Cl_8$	404	–	+

* Only in neutral conditions.

Figure
Click here to download high resolution image

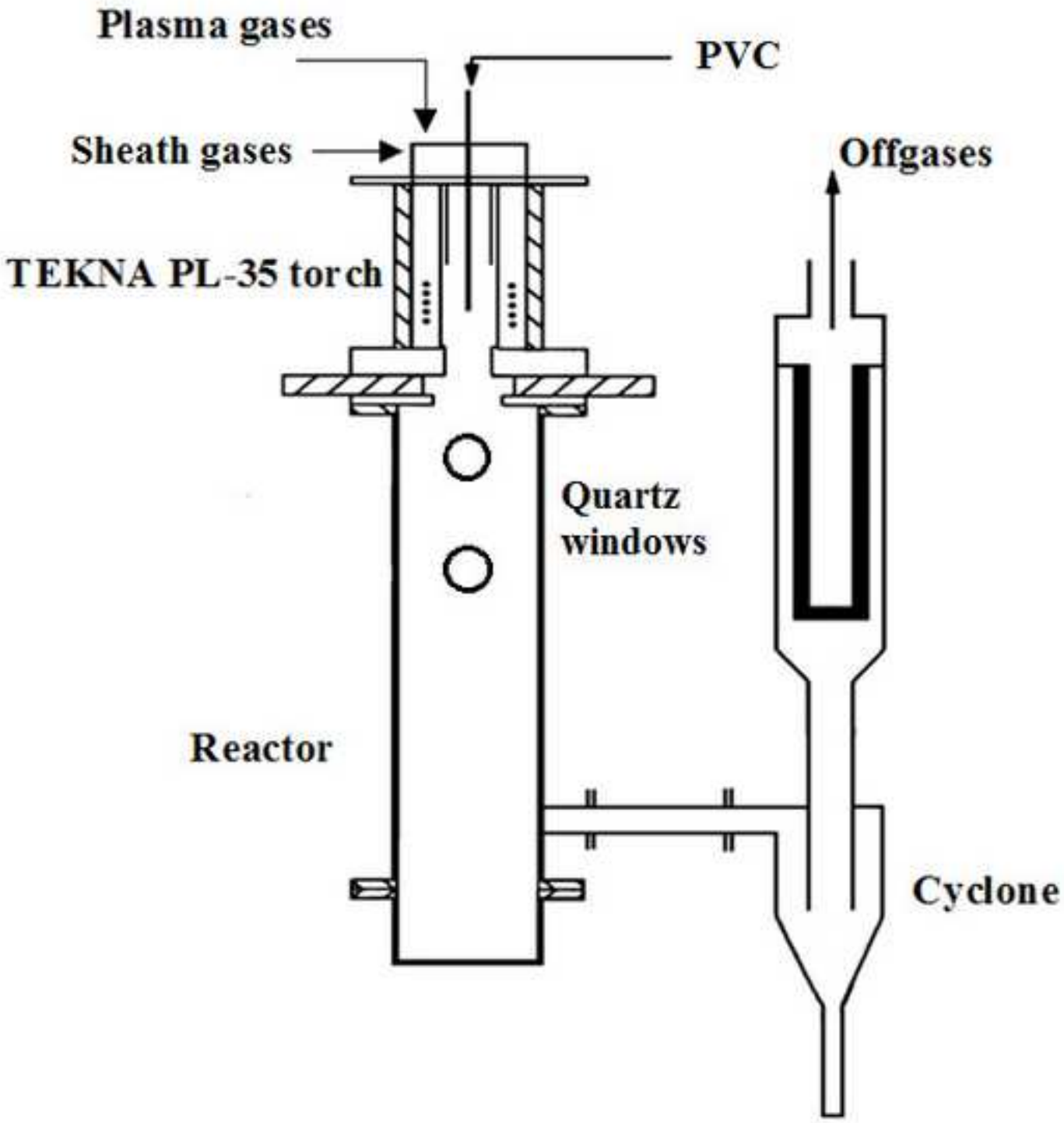

Figure

Click here to download high resolution image

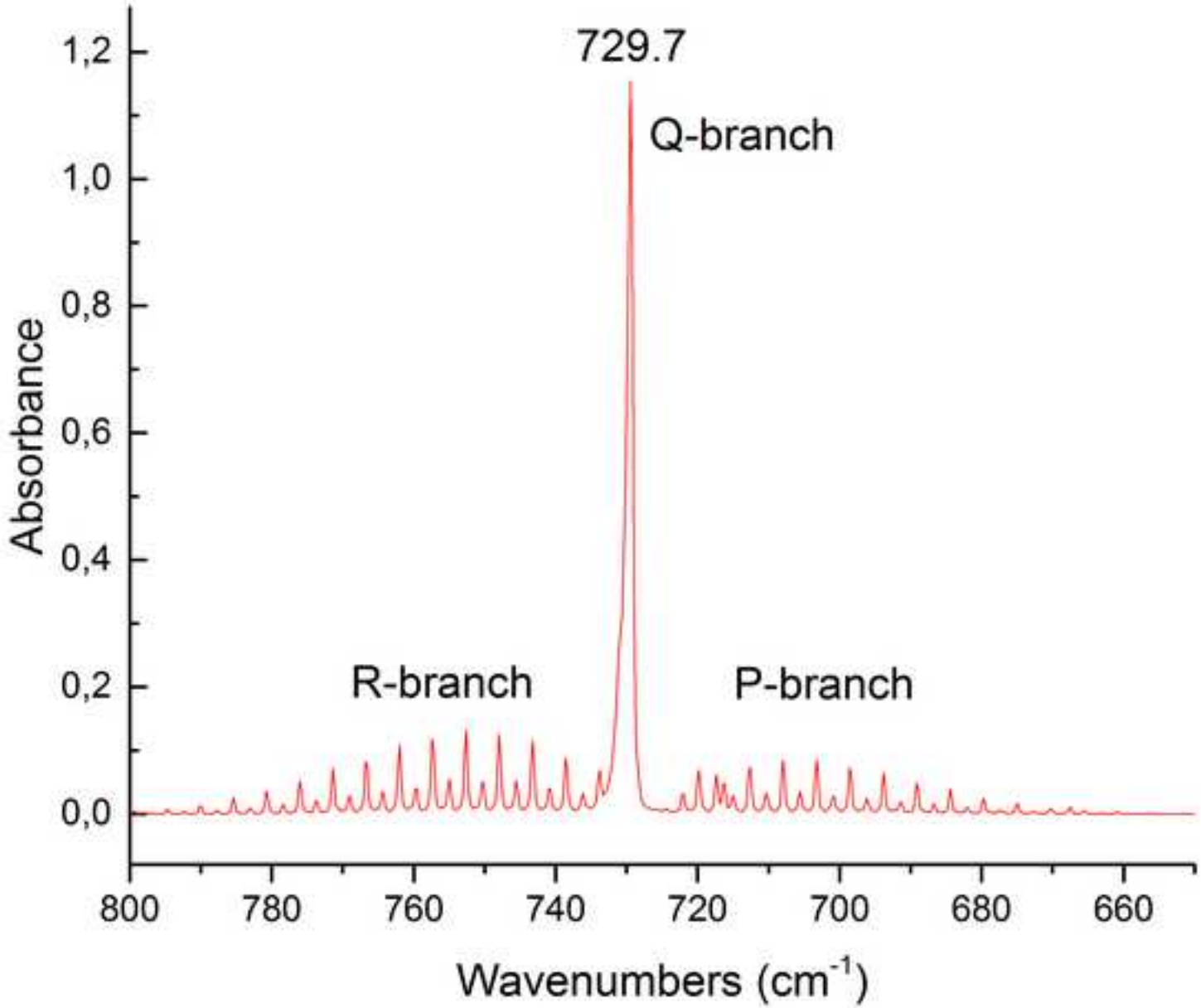

Figure

Click here to download high resolution image

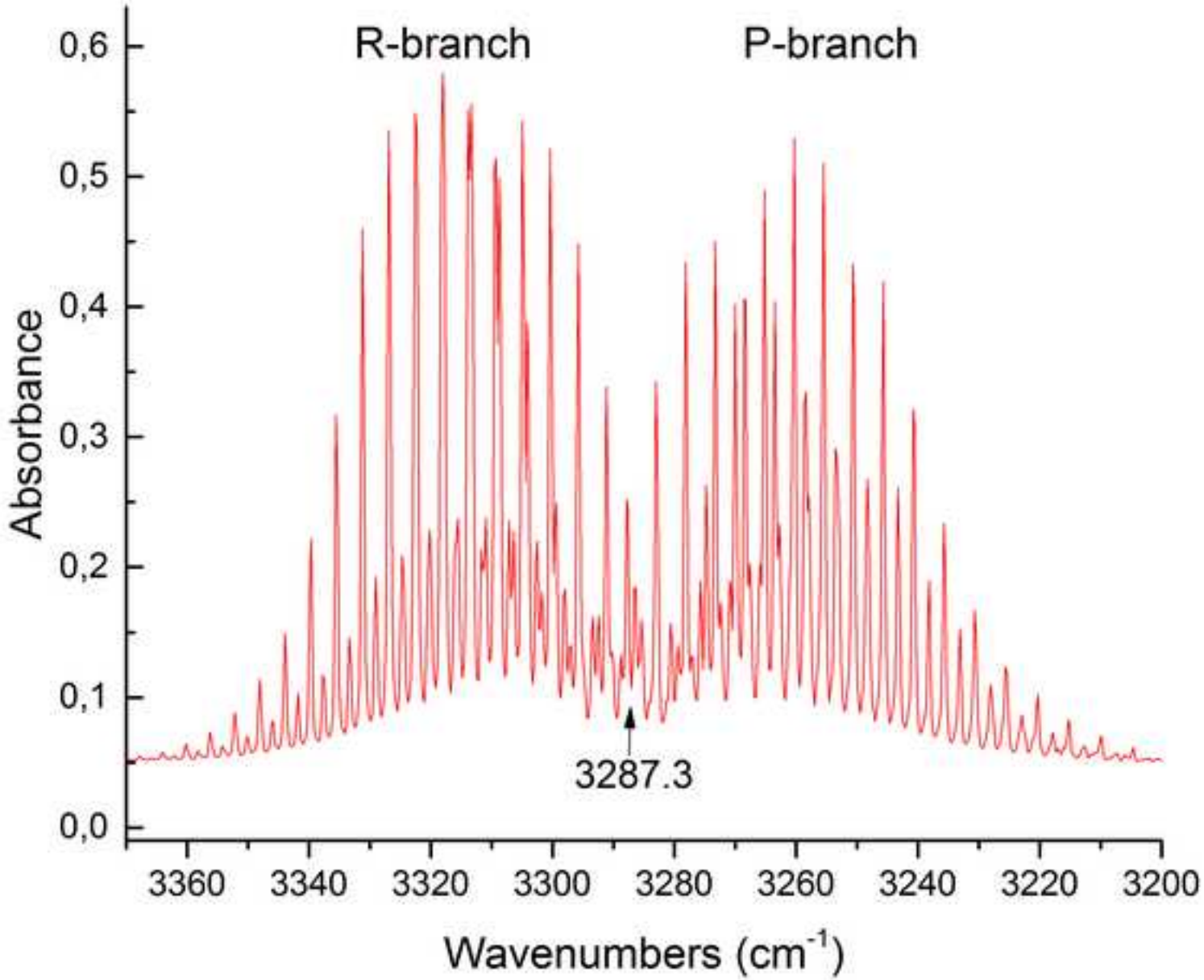

Figure

Click here to download high resolution image

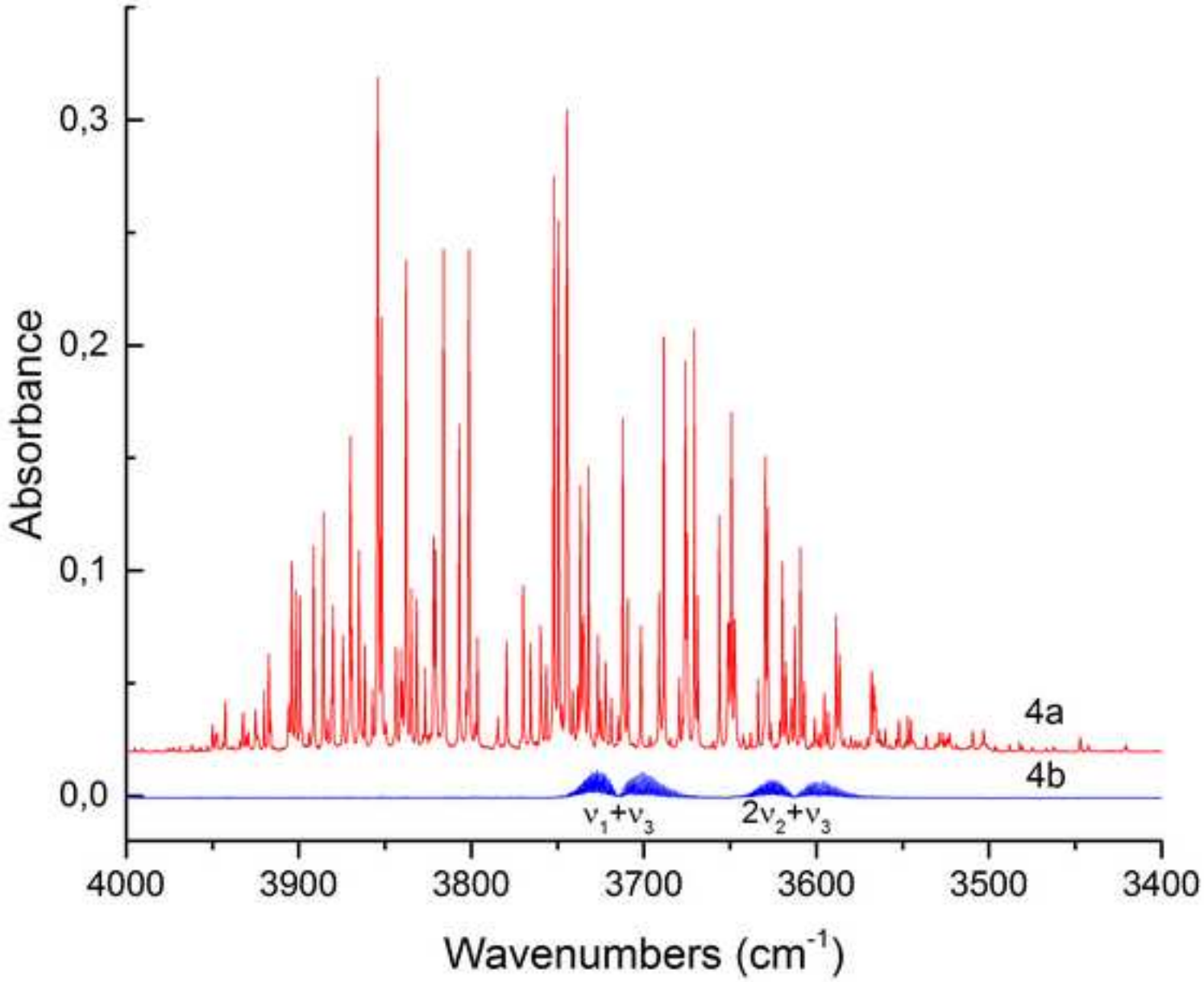

Figure

Click here to download high resolution image

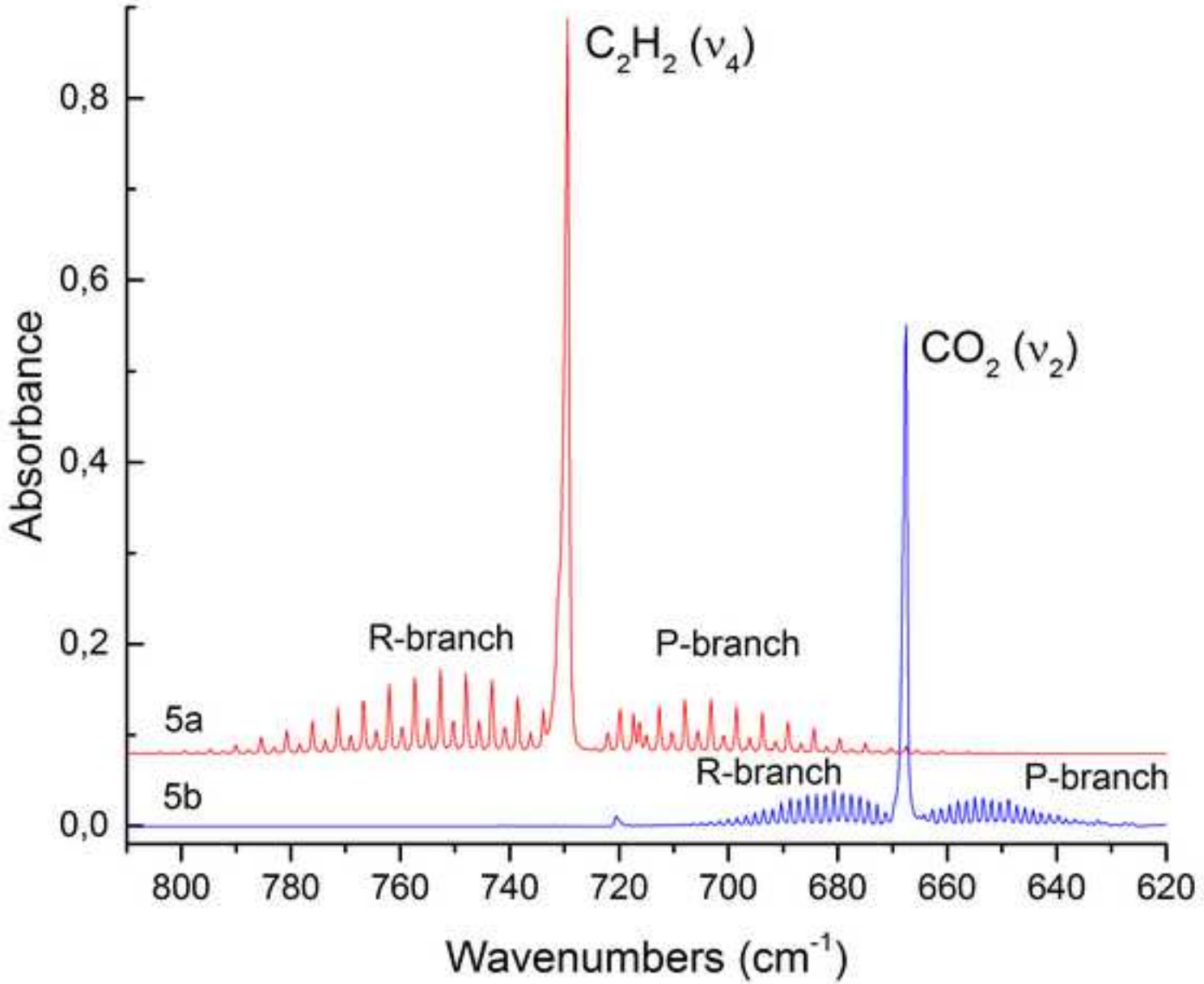

Figure

Click here to download high resolution image

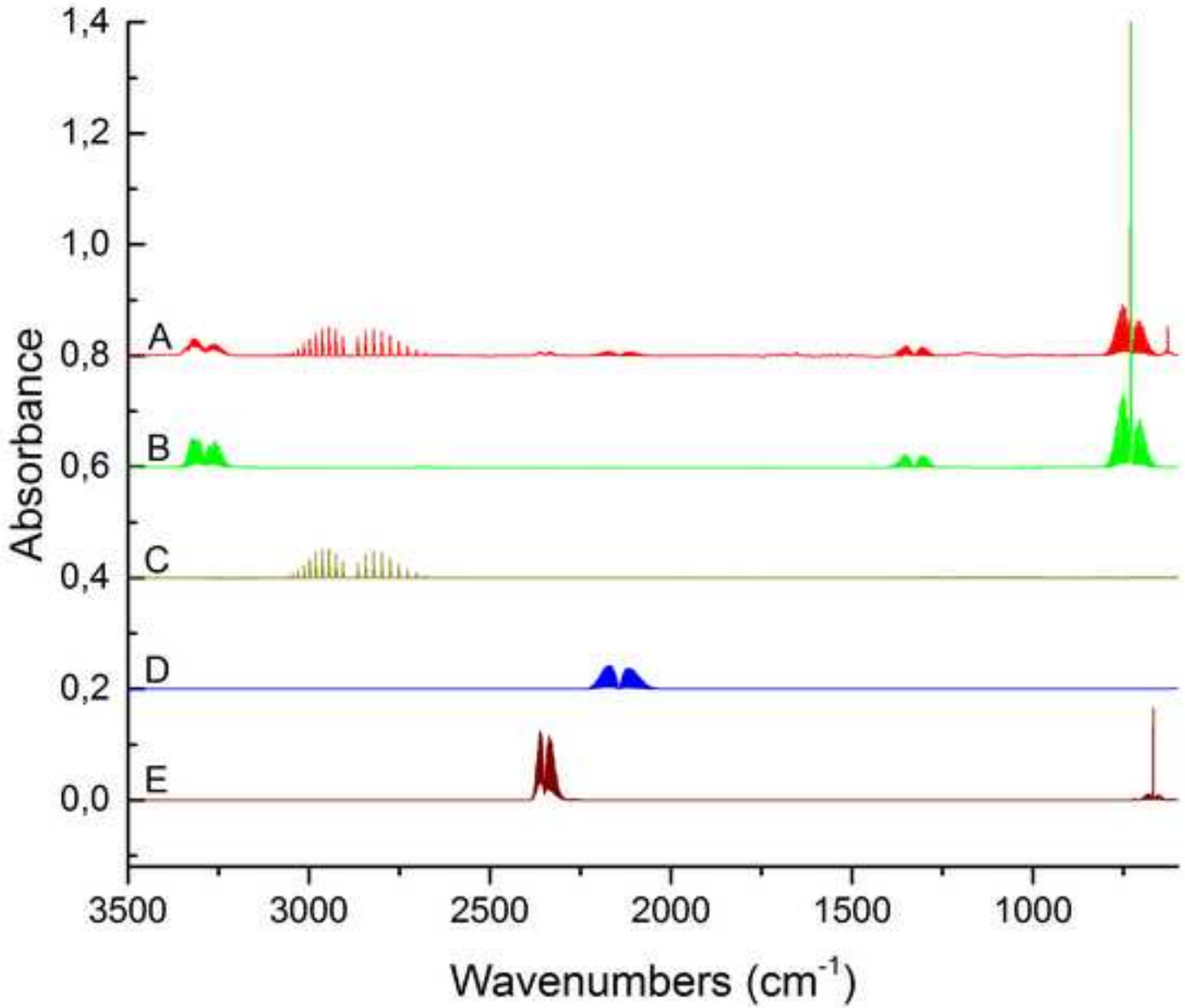

Figure

Click here to download high resolution image

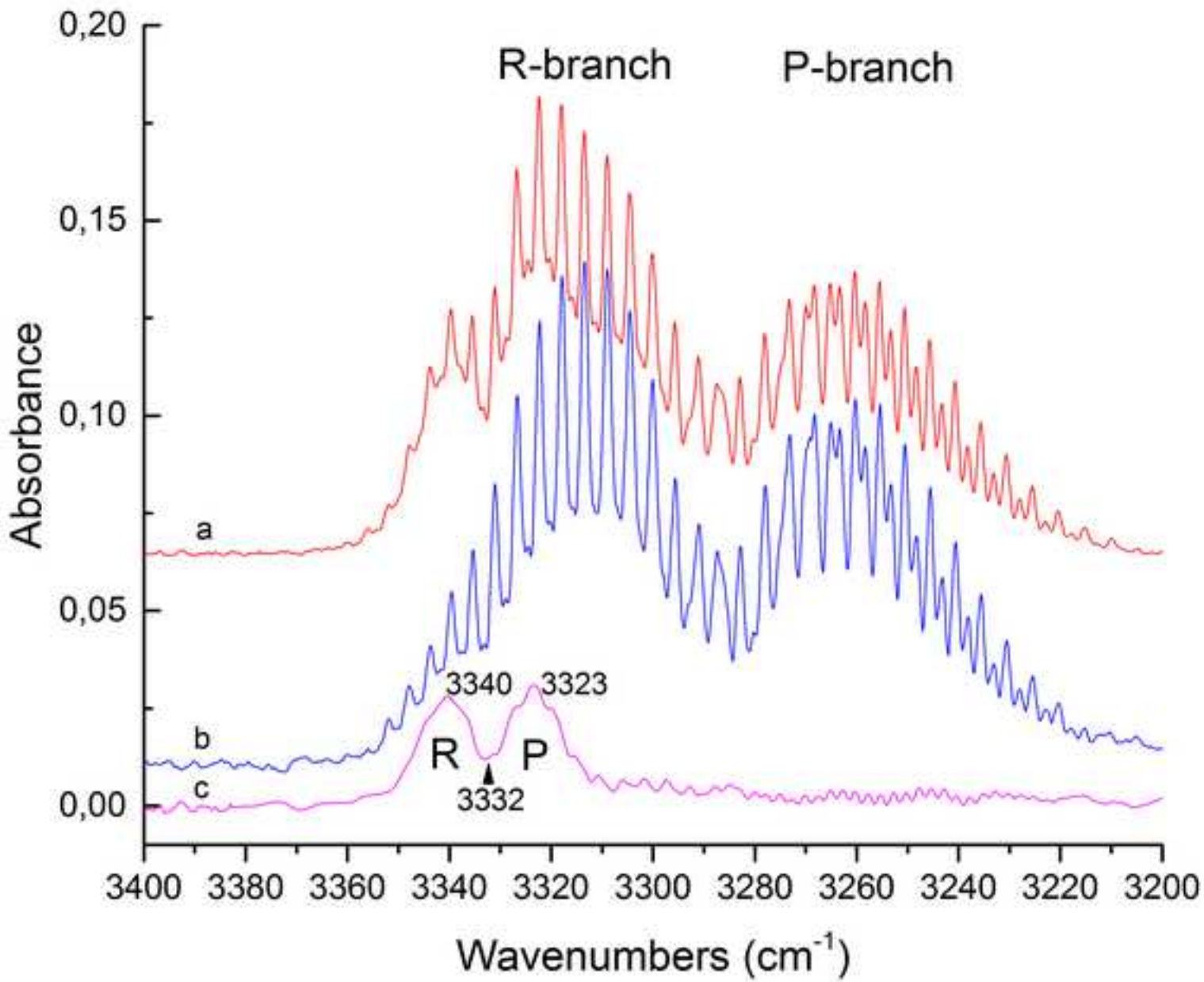

Figure
Click here to download high resolution image

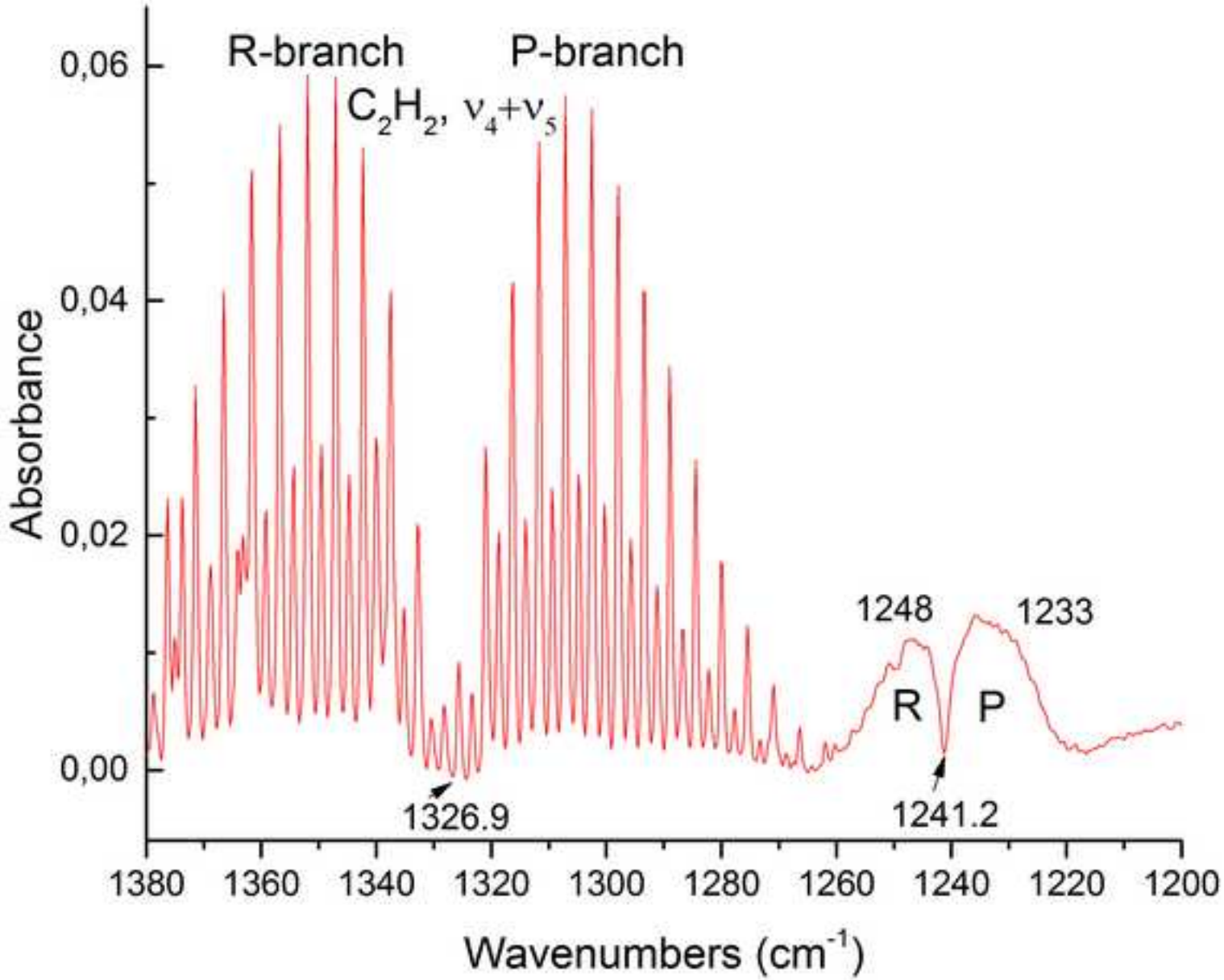

Figure

Click here to download high resolution image

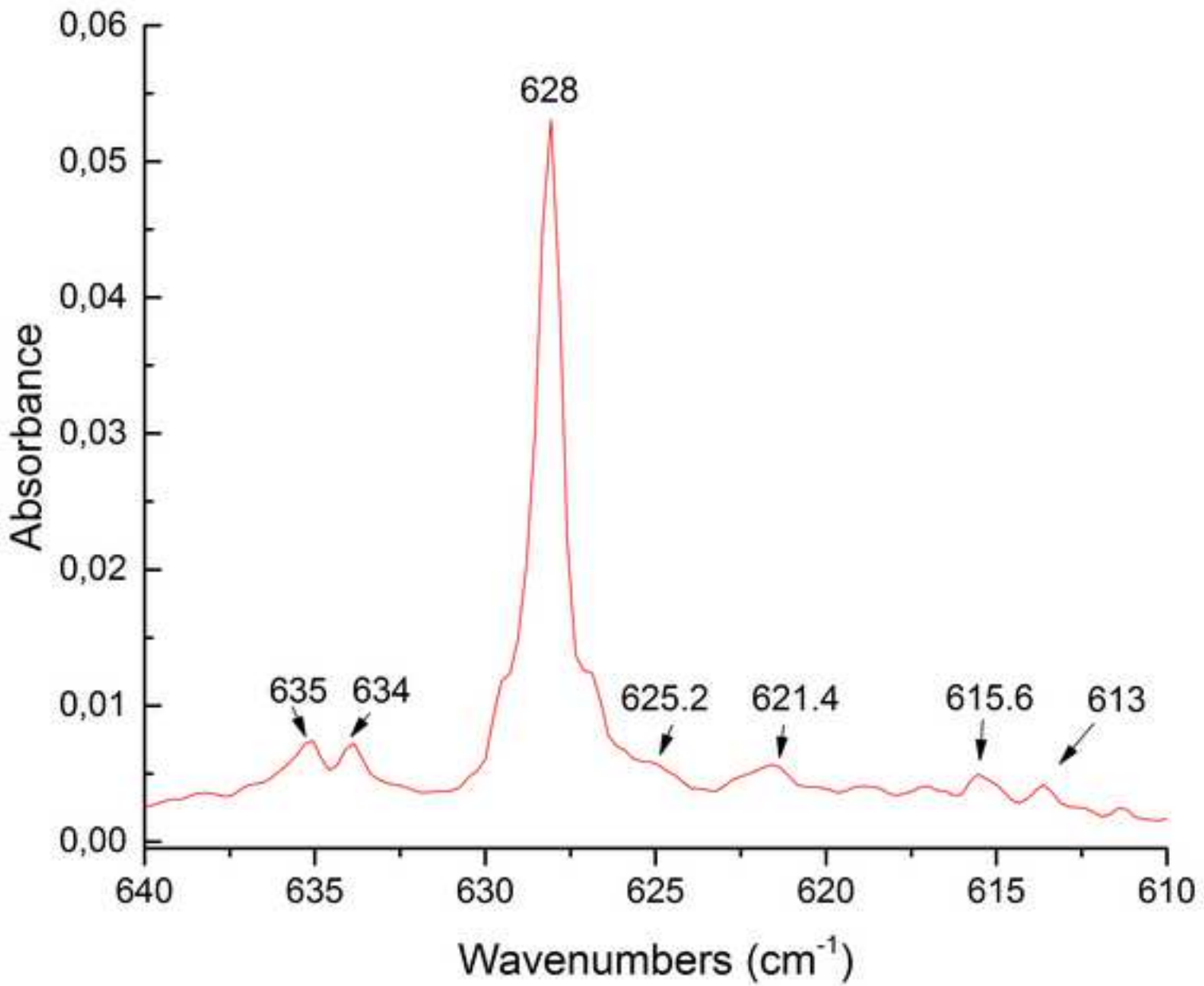

Figure

Click here to download high resolution image

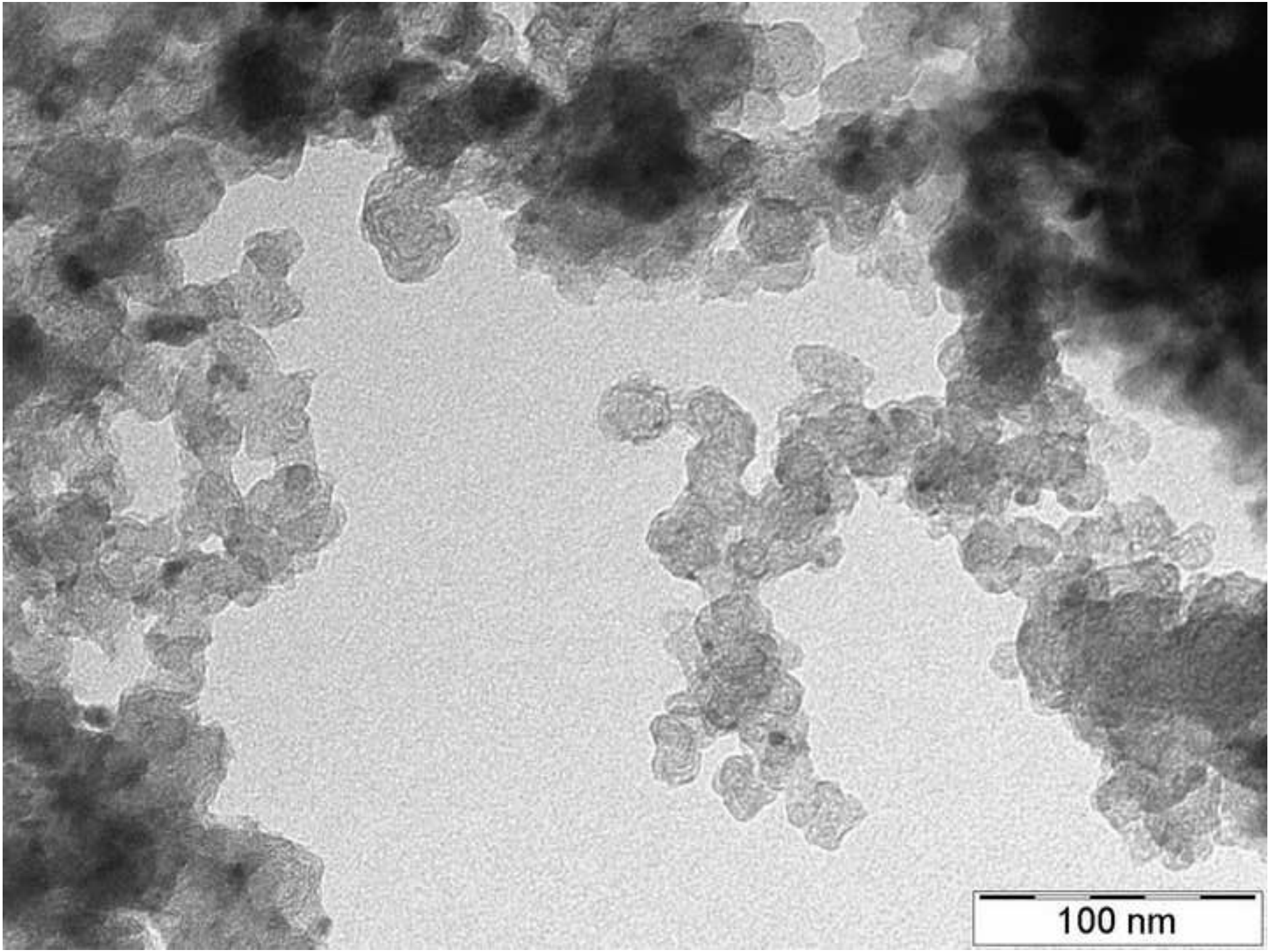

Figure

Click here to download high resolution image

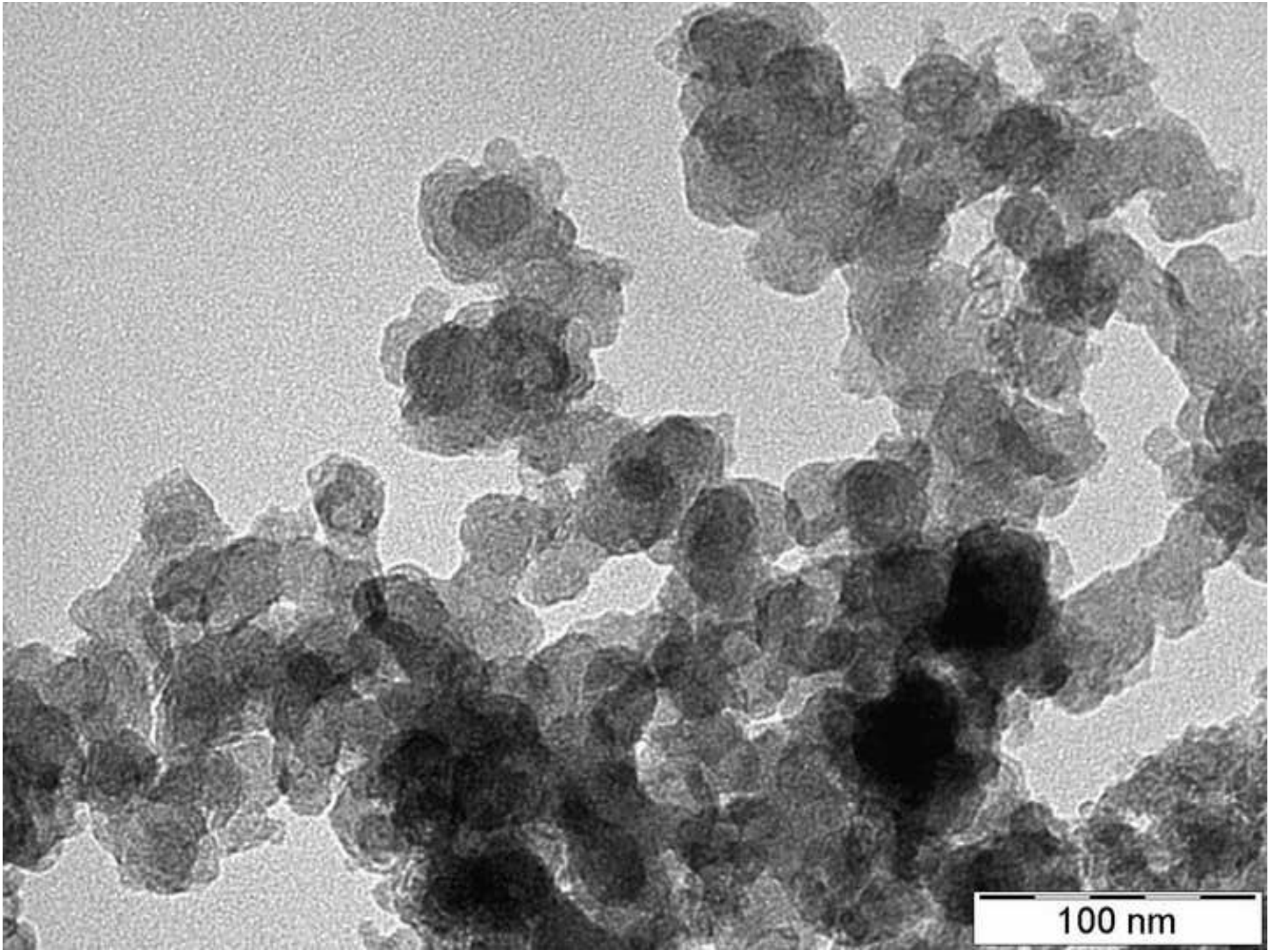

Figure

Click here to download high resolution image

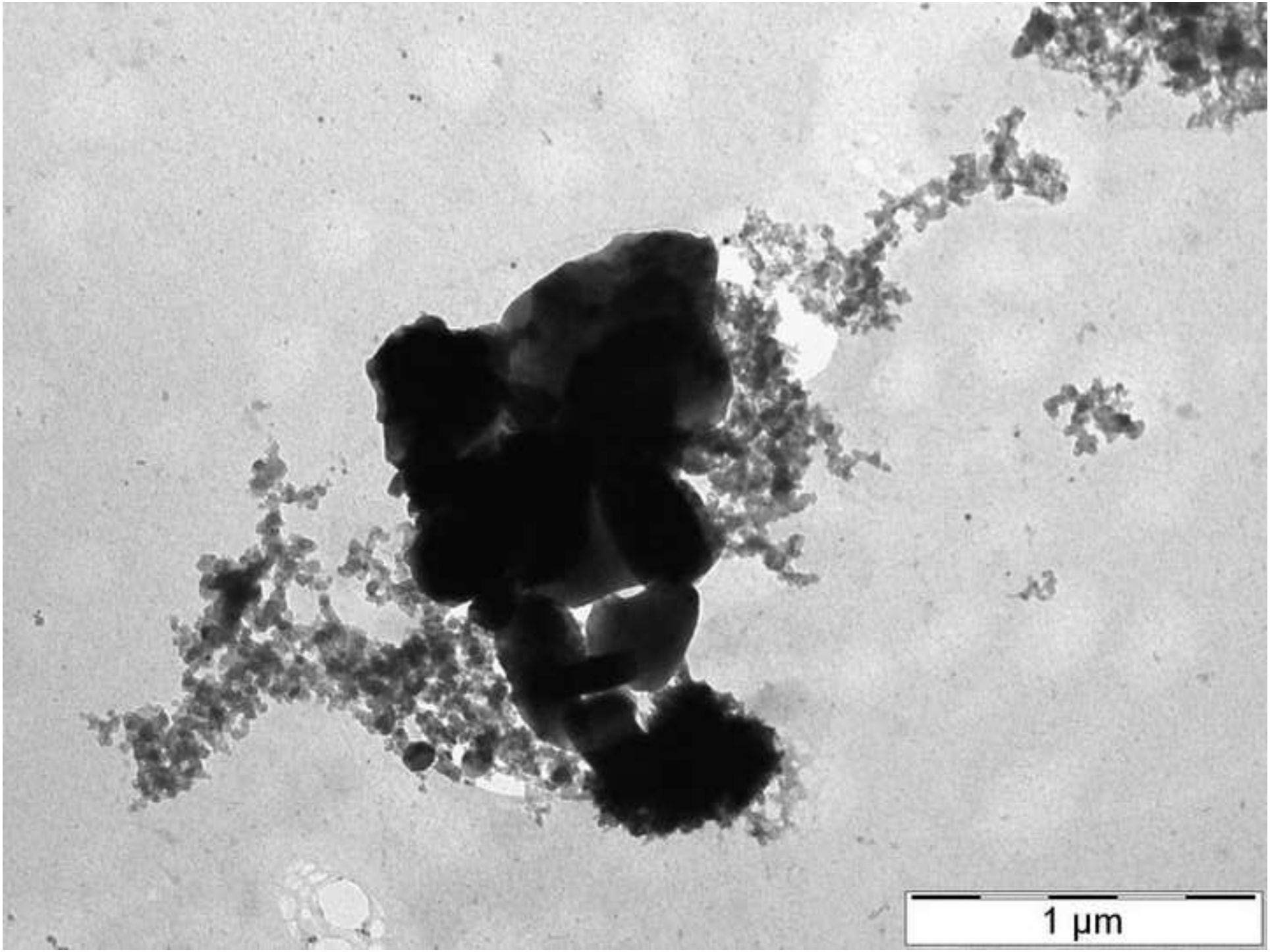

Figure

Click here to download high resolution image

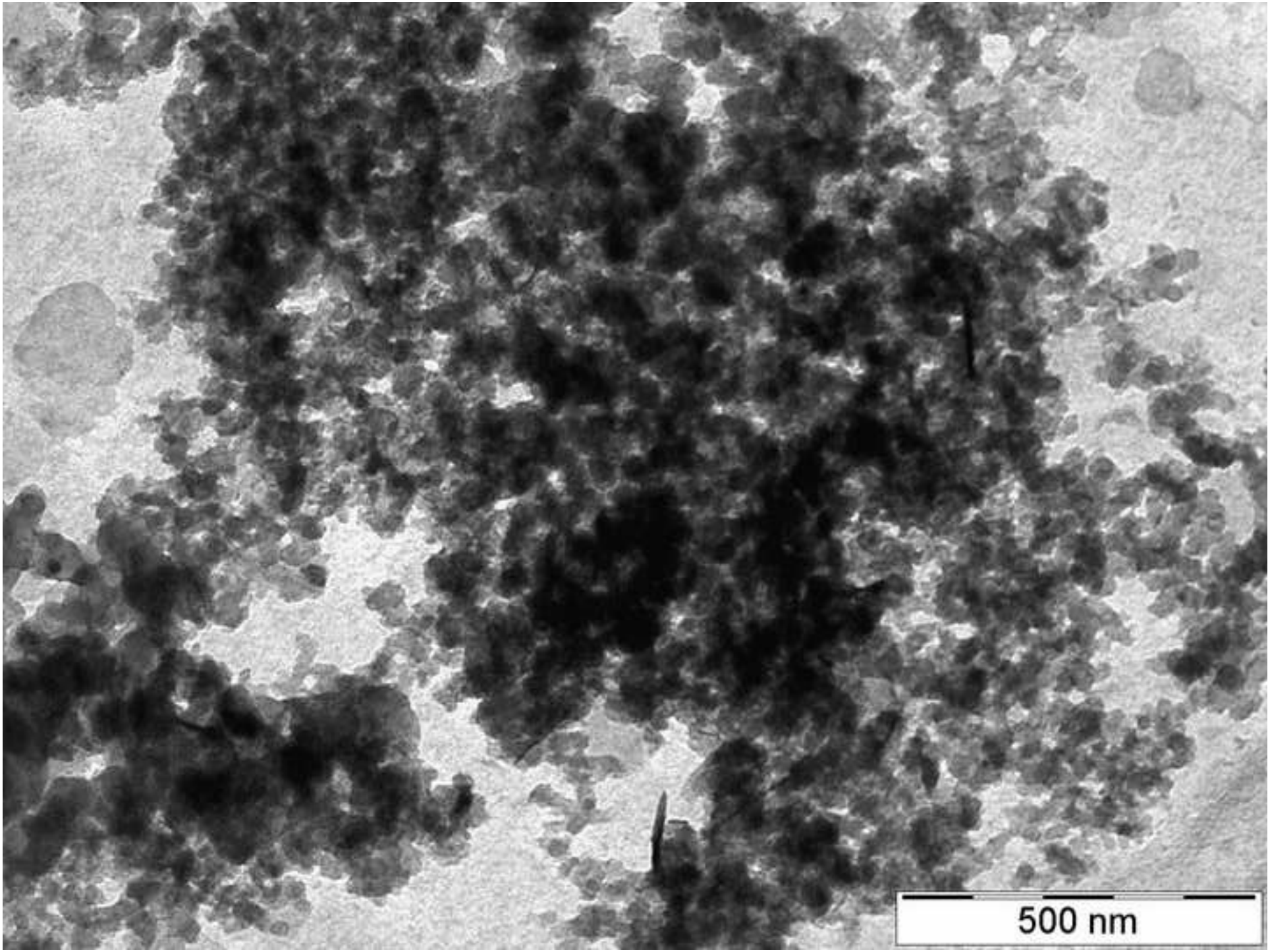

Figure
Click here to download high resolution image

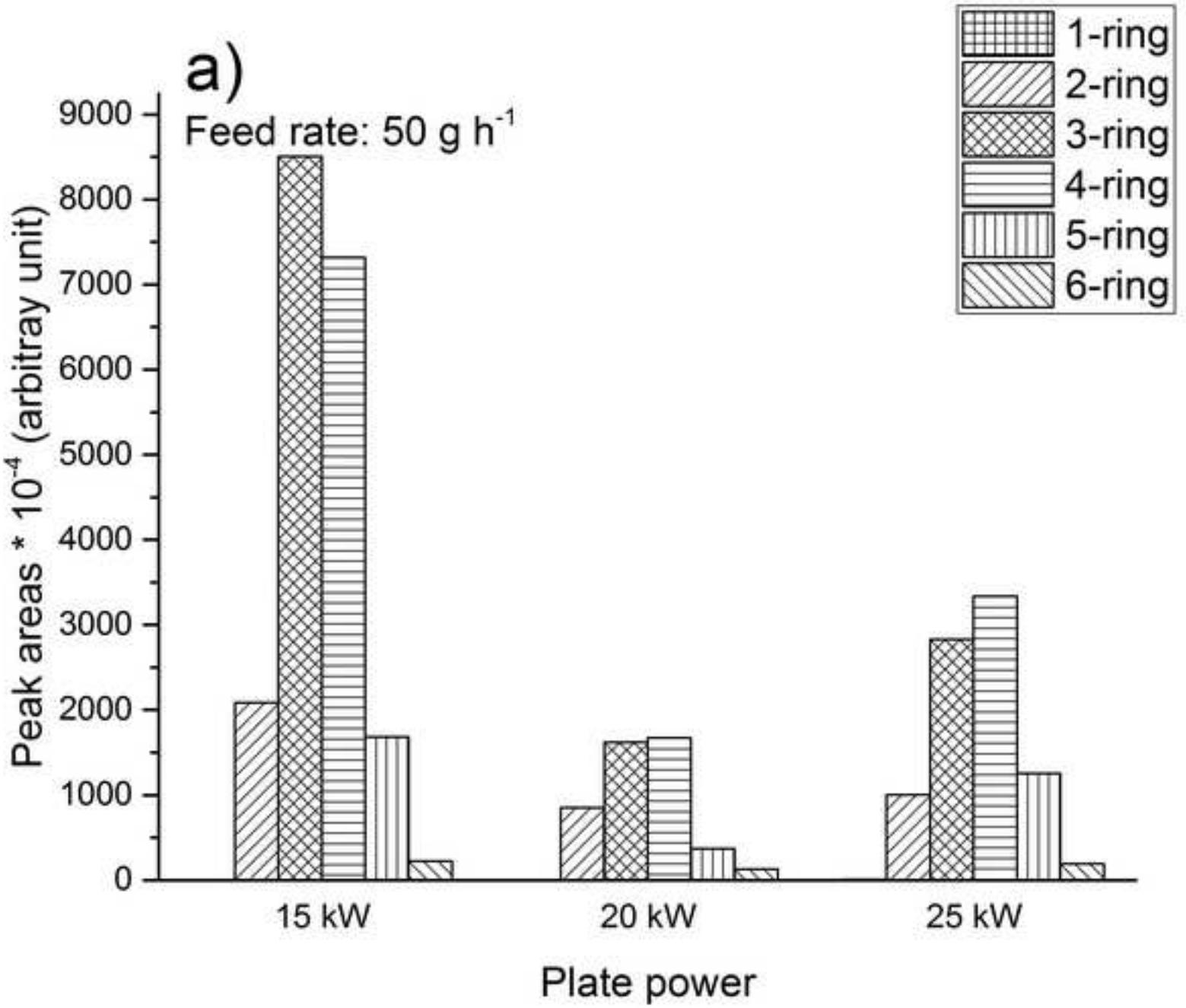

Figure
Click here to download high resolution image

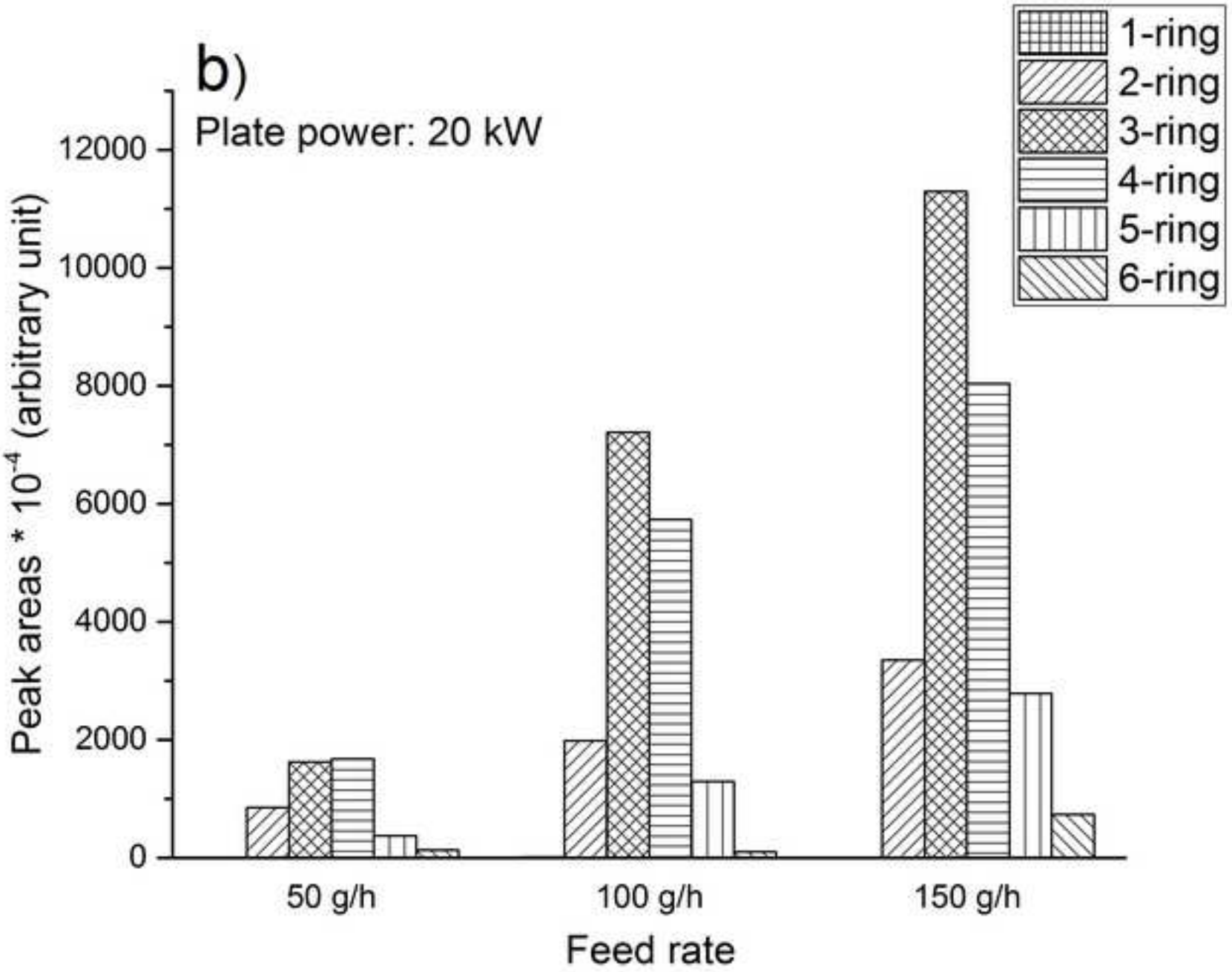

Figure
Click here to download high resolution image

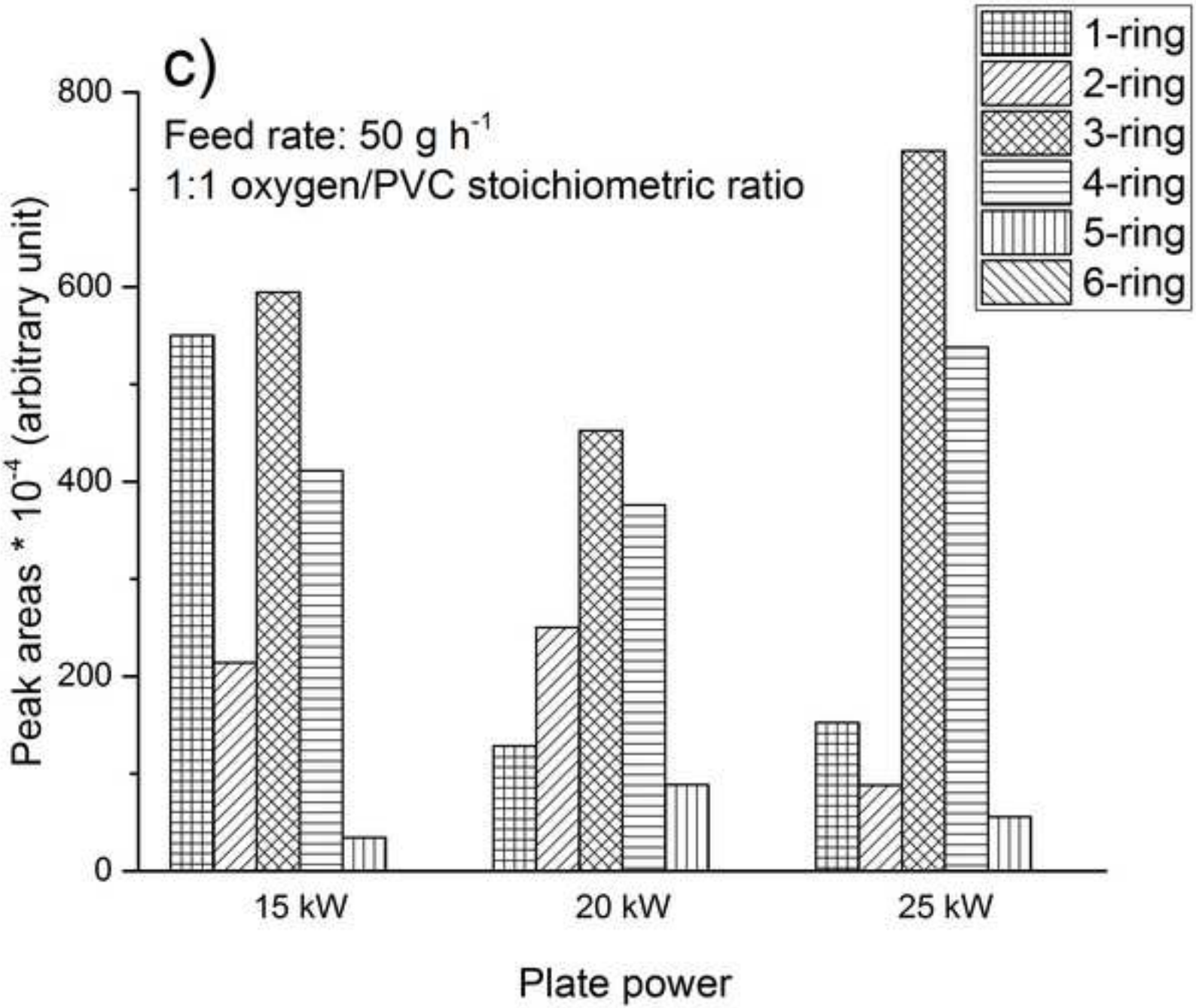

Figure
Click here to download high resolution image

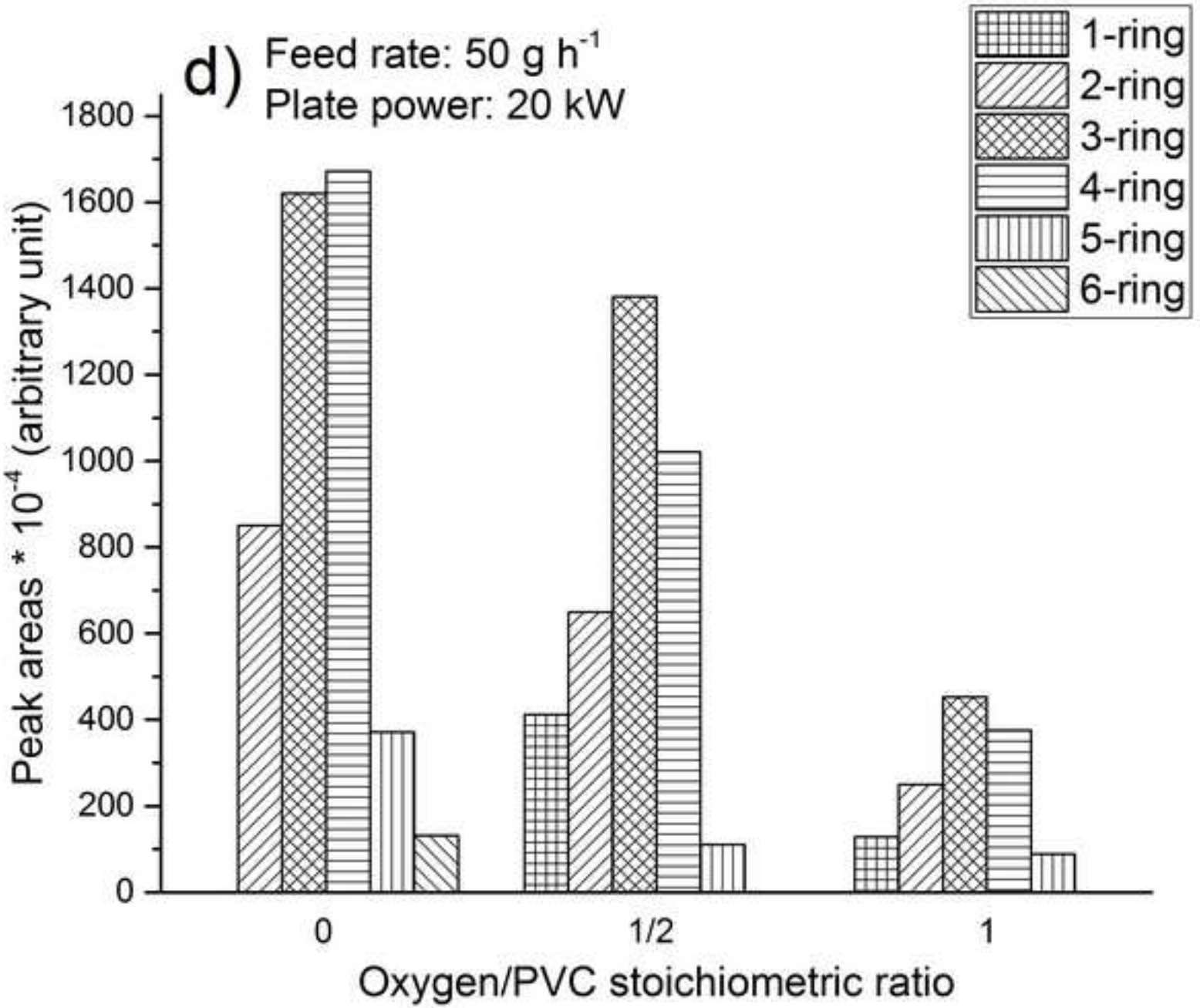

Figure
Click here to download high resolution image

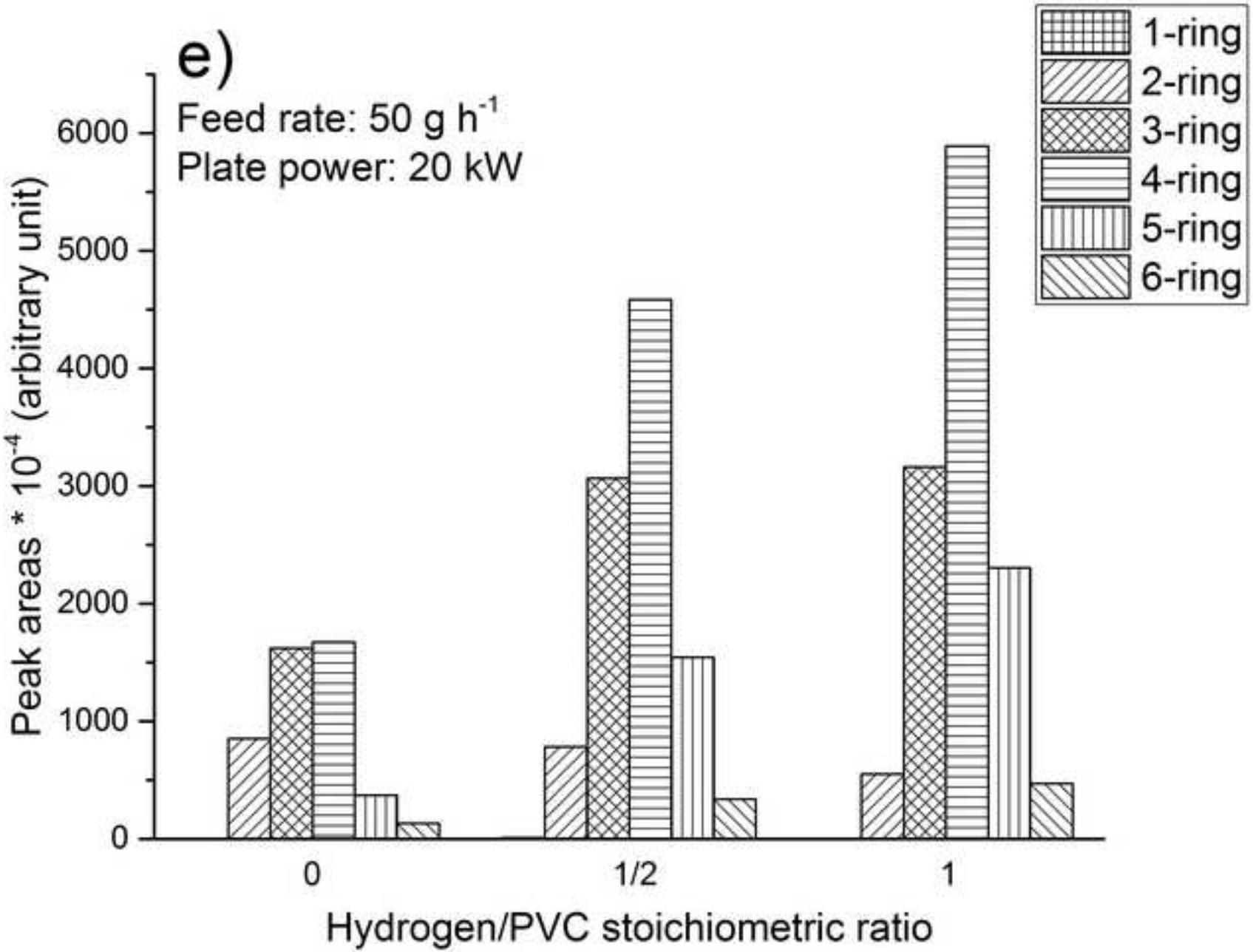

Figure

Click here to download high resolution image